



**HAL**  
open science

# Deriving amplification factors from simple site parameters using generalized regression neural networks: implications for relevant site proxies

Ahmed Boudghene Stambouli, Djawad Zendagui, Pierre-Yves Bard,  
Boumédiène Derras

## ► To cite this version:

Ahmed Boudghene Stambouli, Djawad Zendagui, Pierre-Yves Bard, Boumédiène Derras. Deriving amplification factors from simple site parameters using generalized regression neural networks: implications for relevant site proxies. *Earth Planets and Space*, 2017, 69 (1), 10.1186/s40623-017-0686-3 . hal-01693202

**HAL Id: hal-01693202**

**<https://hal.science/hal-01693202>**

Submitted on 4 Aug 2021

**HAL** is a multi-disciplinary open access archive for the deposit and dissemination of scientific research documents, whether they are published or not. The documents may come from teaching and research institutions in France or abroad, or from public or private research centers.

L'archive ouverte pluridisciplinaire **HAL**, est destinée au dépôt et à la diffusion de documents scientifiques de niveau recherche, publiés ou non, émanant des établissements d'enseignement et de recherche français ou étrangers, des laboratoires publics ou privés.



Distributed under a Creative Commons Attribution 4.0 International License

FULL PAPER

Open Access



# Deriving amplification factors from simple site parameters using generalized regression neural networks: implications for relevant site proxies

Ahmed Boudghene Stambouli<sup>1\*</sup> , Djawad Zendagui<sup>1</sup>, Pierre-Yves Bard<sup>2</sup> and Boumédiène Derras<sup>1</sup>

## Abstract

Most modern seismic codes account for site effects using an amplification factor (AF) that modifies the rock acceleration response spectra in relation to a “site condition proxy,” i.e., a parameter related to the velocity profile at the site under consideration. Therefore, for practical purposes, it is interesting to identify the site parameters that best control the frequency-dependent shape of the AF. The goal of the present study is to provide a quantitative assessment of the performance of various site condition proxies to predict the main AF features, including the often used short- and mid-period amplification factors,  $F_a$  and  $F_v$ , proposed by Borcherdt (in *Earthq Spectra* 10:617–653, 1994). In this context, the linear, viscoelastic responses of a set of 858 actual soil columns from Japan, the USA, and Europe are computed for a set of 14 real accelerograms with varying frequency contents. The correlation between the corresponding site-specific average amplification factors and several site proxies (considered alone or as multiple combinations) is analyzed using the generalized regression neural network (GRNN). The performance of each site proxy combination is assessed through the variance reduction with respect to the initial amplification factor variability of the 858 profiles. Both the whole period range and specific short- and mid-period ranges associated with the Borcherdt factors  $F_a$  and  $F_v$  are considered. The actual amplification factor of an arbitrary soil profile is found to be satisfactorily approximated with a limited number of site proxies (4–6). As the usual code practice implies a lower number of site proxies (generally one, sometimes two), a sensitivity analysis is conducted to identify the “best performing” site parameters. The best one is the overall velocity contrast between underlying bedrock and minimum velocity in the soil column. Because these are the most difficult and expensive parameters to measure, especially for thick deposits, other more convenient parameters are preferred, especially the couple  $(V_{s30}, f_0)$  that leads to a variance reduction in at least 60%. From a code perspective, equations and plots are provided describing the dependence of the short- and mid-period amplification factors  $F_a$  and  $F_v$  on these two parameters. The robustness of the results is analyzed by performing a similar analysis for two alternative sets of velocity profiles, for which the bedrock velocity is constrained to have the same value for all velocity profiles, which is not the case in the original set.

**Keywords:** 1D linear site response, Site proxies, Amplification factors, Neural network

\*Correspondence: stambouli\_ahmed@yahoo.fr

<sup>1</sup> Risk Assessment and Management Laboratory (RISAM), Faculté de Technologie, Université Abou Bekr Belkaid, BP 230-13048, Tlemcen, Algeria

Full list of author information is available at the end of the article

## Introduction

It is recognized that site effects have a great impact on seismic ground motion and could thus cause increased damage to structures. For instance, during the Michoacan Earthquake of Mexico (e.g., Anderson et al. 1986; Hall and Beck 1986; Esteva 1988; Singh et al. 1988a, b; Bard et al. 1988; Romo et al. 1988; Seed et al. 1988; Sanchez-Sesma et al. 1988; Kawase and Aki 1989; Singh and Ordaz 1993; Chávez-García and Bard 1994; Cruz-Atienza et al. 2016) amplification induced from site effects has been recognized as the major cause of structural collapse.

In this study, seismic amplification is measured with an amplification factor (AF), defined as the ratio of response spectra between soil surface and outcropping reference rock. Among many other parameters characterizing the intensity of ground motion, response spectra are the most used in engineering practice. Most building codes use response spectra to define design earthquake loads on engineered structures. Most hazard assessment studies use acceleration response spectra to define the seismic motion through ground motion prediction equations (GMPEs) that correlate the spectral ordinates to magnitude, distance, and site parameters. In most GMPEs, the site conditions are described with a single-site proxy; currently, the most common is the “ $V_{s30}$ ” parameter, corresponding to the harmonic average of S-wave velocity over the top 30 m, first introduced by Borchardt (1994), which has, since then, been widely used (see, for instance, Martin and Dobry 1994; Dickenson and Seed 1996; Dobry et al. 2000; Rodríguez-Marek et al. 2001; Pitilakis et al. 2001). Almost all recent GMPEs, for instance, the NGA (Abrahamson et al. 2008), NGAWest2 (Gregor et al. 2014; Ancheta et al. 2014), and GMPEs derived from the RESORCE database (Douglas et al. 2014) still rely on  $V_{s30}$  to describe site conditions. It is sometimes complemented or replaced by other site parameters, such as the fundamental frequency  $f_0$  (Castellaro et al. 2008; Luzi et al. 2011; Cadet et al. 2012; Pitilakis et al. 2012, 2013) or depth to a hard bedrock level defined with a threshold velocity (from 1 to 2.5 km/s; see Ancheta et al. 2014). The terms associated to such site proxies provide a mechanism for quantifying the frequency-dependent “amplification factor” with respect to “standard rock” (usually characterized by  $V_{s30} = 760$  to 800 m/s). The same proxies are also used in regulatory codes to tune the characteristics of design spectra, i.e., peak ground acceleration (PGA), plateau bandwidth and level, and long-period decay, to the site conditions. For instance, this is the case for the major building codes used at the international level, i.e., International Building Code (IBC 2012), Uniform Building Code (UBC 1997), and Eurocode 8 (EC8 2004).

However, these site proxies are too simple and too few to capture the entire physics of site amplification, and distinct sites with similar site proxy values (e.g.,  $V_{s30}$ ) could have different amplification characteristics. This has at least two consequences. First, it significantly impacts the aleatory variability of GMPEs by increasing the within-event term, which in turn increases the hazard estimates, especially at long return periods. Second, corresponding site terms may exhibit significant variations from one GMPE to another, depending on the strong motion data used for their derivation. For instance, the relationship between  $V_{s30}$  and deeper velocity structure is not identical in the Los Angeles basin, Japanese coastal plains, or intra-mountain basins in the Alps or the Apennines; therefore, the associated long- or short-period effects may differ. The issue addressed in this paper is to identify the best site parameters that optimally explain, and therefore predict, the actual site-specific amplification factor. The aim is to derive “stand-alone” site terms, which could be applied as a post-processing step to any rock GMPEs.

With that aim in mind, the focus here is on the 1D response of horizontally stratified soil columns, and on investigating the relationships between corresponding amplification factors on response spectra, and limited number of “site proxies” describing the overall characteristics of the soil profile. A series of 858 real soil profiles are considered, and their linear viscoelastic responses to vertically incident S waves are computed for 14 distinct, real input waveforms spanning a wide range of frequency contents. For each site, the geometric average amplification factor is derived from these 14 different loadings, and an artificial neural network approach is used to investigate the correlation between this average amplification factor and various sets of soil characteristics. Sensitivity studies are performed to identify the relative performance of several site proxies, with the goal of proposing optimal combination sets offering a good compromise between physical relevancy and practical affordability. The robustness of the results is tested by conducting the same analysis on two additional sets of soil profiles, termed normalized soil profiles (NP) and truncated soil profiles (TP), modified to correspond to a uniform bedrock velocity of 800 m/s.

## Derivation of amplification factors (AF)

### Introduction

This section describes the overall procedure to obtain a set of amplification factors for several hundreds of realistic soil profiles. For a particular soil profile and input motion, the amplification factor is computed as the ratio of response spectra at the soil surface to response spectra at the outcropping reference rock.

$$AF(T) = \frac{SA(T)_s}{SA(T)_b} \quad (1)$$

where  $SA(T)_s$  and  $SA(T)_b$  are, respectively, the 5% response spectra at the site surface and outcropping reference bedrock, while  $T$  is the structural period. They are obtained as follows:

1. Choose a soil profile  $S$  and use the 1D viscoelastic analysis to derive the corresponding Fourier transfer function  $T(f)$
2. Select a reference rock motion  $b(t)$  and compute its Fourier transform  $B(f)$  together with its 5% acceleration response spectrum  $SA(T)_b$
3. Compute the Fourier transform of motion at the soil surface  $A_s(f)$  by multiplying  $B(f)$  by  $T(f)$
4. Perform an inverse Fourier transform on  $A_s(f)$  to obtain the surface motion in time domain  $a_s(t)$ .
5. Derive the 5% acceleration response spectrum  $SA(T)_s$  from  $a_s(t)$ .

Once  $SA(T)_s$  and  $SA(T)_b$  are derived, the amplification factor for site  $s$  and input  $b$  can be readily obtained from Eq. (1).

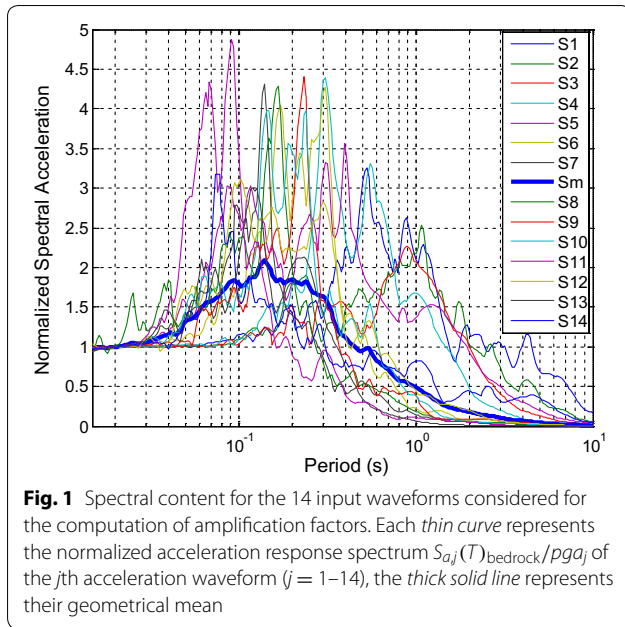
The next sections provide additional information for selected input accelerograms, followed by a short indication on the way transfer functions, and thus, amplification factors are computed using classical concepts of wave propagation in horizontally stratified media. The considered site profiles are finally briefly described, from original soil profile information to selecting a small number of site proxies, and providing their statistical distribution to assess the relevancy and validity domain of the study.

#### Seismic input $SA(T)_b$

Fourteen input waveforms (S1–S14), recorded on outcropping rock, are selected from the RESORCE database (Akkar et al. 2014). Their characteristics are listed in Table 1. The amplification factor defined in Eq. (1) depends on the frequency content of the seismic motion (see, for instance, Biro and Renault 2012; Renault et al. 2014; Bora et al. 2015, 2016). Therefore, it was decided to select real accelerograms, corresponding to near-source rock recordings, with a wide range of spectral contents, and derive the geometrical mean of the amplification factors obtained for each accelerogram. As illustrated in Fig. 1, the spectral

**Table 1 Main characteristics of the 14 reference acceleration time histories**

Identification	RESORCE Waveform Id	PGA (m/s <sup>2</sup> )	Earthquake	Station	Mw	Distance	Site conditions	Peak frequency (highest PSA)
S1	16,149	1.269	Manjil (Iran) 20/06/1990	Zanjan	7.7	56	A	$f < 2$ Hz
S2	16,351	1.288	Olfus (Iceland) 29/05/2008	Ljosafoss-Hydroelectric Power Station	6.1	11	A	$f < 2$ Hz
S3	16,352	3.190	Olfus (Iceland) 29/05/2008	Selfoss City Hall	6.1	3	A	$f < 2$ Hz
S4	15,537	2.074	South Iceland 17/06/2000	Thjorsarbru	5.0	10	A	$2 \text{ Hz} < f < 4$ Hz
S5	6756	3.106	South Iceland 17/06/2000	Flagbjarnarholt	6.6	15	A	$2 \text{ Hz} < f < 4$ Hz
S6	6765	3.140	South Iceland 17/06/2000	Thjorsarbrun	6.6	4	A	$2 \text{ Hz} < f < 4$ Hz
S7	583	1.003	Lazio-Abruzzo 11/05/1984	Villetta Barrea	5.3	2	A	$4 \text{ Hz} < f < 8$ Hz
S8	16,974	1.474	L'Aquila 07/04/2009 (aftershock)	Pescomaggiore	5.3	10	A	$4 \text{ Hz} < f < 8$ Hz
S9	15,905	3.006	Firouzabad (Iran) 20/06/1994	Zarrat	5.8	11	A	$4 \text{ Hz} < f < 8$ Hz
S10	188	1.496	Basso Tirenno 15/04/19878	Naso	5.5	16	A	$4 \text{ Hz} < f < 8$ Hz
S11	17,116	1.023	L'Aquila aftershock 09/04/2009	Montereale	4.9	10	A	$8 \text{ Hz} < f < 16$ Hz
S12	6802	4.260	South Iceland aftershock 21/06/2000	Thjorsartun	6.4	3	A	$8 \text{ Hz} < f < 16$ Hz
S13	16,996	1.393	L'Aquila aftershock 07/04/2009	L'Aquila Via Aterna—Il Moror	4.2	2	A	$8 \text{ Hz} < f < 16$ Hz
S14	6789	0.803	South Iceland aftershock 21/06/2000	Hveragerdi-Church	6.4	23	A	$8 \text{ Hz} < f < 16$ Hz

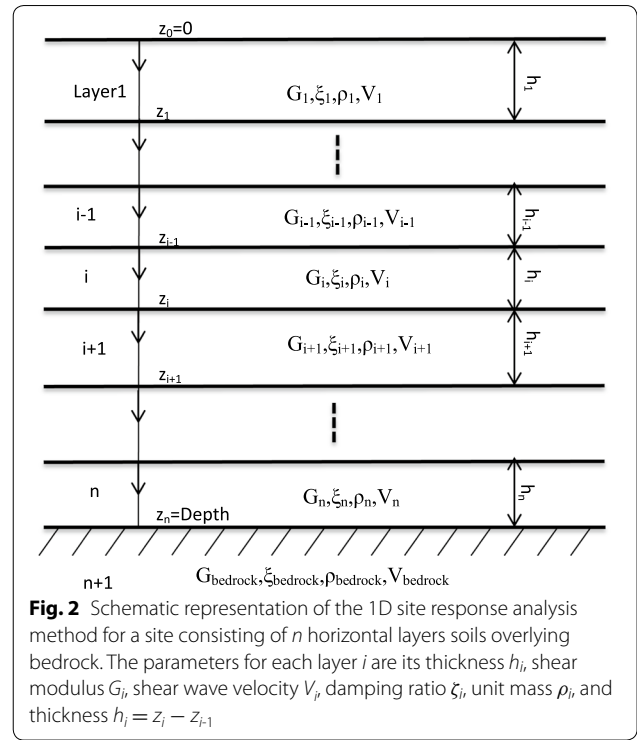


shapes corresponding to each selected accelerogram, i.e., the response spectra normalized by the corresponding PGA, exhibit peak periods ranging from 0.07 s to slightly beyond 1 s, with four motions with peak periods in the range [0.0625–0.125 s], four in the range [0.125–0.25 s], three in the range [0.25–0.5 s], and three >0.5 s. The corresponding PGA values are also listed in Table 1 (ranging from 0.8 to 4.2 m/s<sup>2</sup>), but actual PGA values have no importance in the present computations because only the linear response is considered. The main goal is to ensure a representative average amplification factor that is unbiased by spectral contents too rich in either short or long periods.

**Theoretical derivation of the transfer function  $T(f)$**

For a particular soil profile, the AF is computed once the transfer function  $T(f)$  is known. In this study, 1D viscoelastic soil behavior is considered. The soil is ideally composed of  $n$  horizontally layered soils deposit resting on a substratum that is termed bedrock (see Fig. 2). Each layer  $i$  is fully known by its thickness  $h_i$ , shear modulus  $G_i$  or shear wave velocity  $V_i$ , damping ratio  $\zeta_i$ , and mass density  $\rho_i$ . The underlying half-space has a shear wave velocity  $V_{n+1}$  that is termed  $V_{\text{bedrock}}$ . The vertical  $z$ -axis is oriented downwards, and its origin is taken at the free surface. The top of each layer  $i$  is located at the depth  $z_{i-1}$ , and its bottom at depth  $z_i = z_{i-1} + h_i$ . The response of the soil column to harmonic, vertically incident plane shear waves is governed by the equation (Kramer 1996):

$$(1 + 2i \zeta_i) \frac{\partial^2 u_i}{\partial z^2} = -\frac{\omega^2}{V_i^2} u_i \tag{2}$$



where  $u_i$  is the horizontal displacement in the  $i$ th layer,  $\omega$  is the angular frequency, and  $\zeta_i$  is the damping ratio.

In each layer, the wave field can be described as the summation of an up-going and a down-going plane wave with unknown amplitudes  $A_i$  and  $B_i$ . Solving the stress and displacement continuity equations at each interface establishes the relationships between these amplitudes for two adjacent layers. These relationships can thus be propagated from the bottom (unit up-going amplitude) to top layer. Using the free surface condition, the wave amplitudes in the top layer can be derived, and the transfer function with respect to the motion at outcropping bedrock.

$$u_i(z, \omega) = \left[ A_i e^{i\omega(z-z_{i-1})/V_i} + B_i e^{-i\omega(z-z_{i-1})/V_i} \right] e^{i\omega t} \tag{3}$$

$$T(f) = u_1(z = 0, \omega)/2 = A_1 \tag{4}$$

Since the pioneering work of Thomson (1950) and Haskell (1953), many codes such as SHAKE (Schnabel et al. 1973), DEEPSOIL (Hashash et al. 2012), or EERA (Bardet et al. 2000) have been developed that provide the transfer function in the linear domain. However, we developed our own MATLAB® code and verified its accuracy against DEEPSOIL and EERA.

In addition, the damping is estimated in relation to the quality factor  $Q_{Si}$  using the well-known equation:



$$\zeta_i = \frac{1}{2Q_i} \quad (5)$$

The S-wave quality factor  $Q_i$  is estimated here as related to the S-wave velocity through a scaling factor  $SC_Q$ , as described in Aki and Richards (1980) and Fukushima et al. (1995):

$$Q_{Si} = V_i/SC_Q \quad (6)$$

where  $SC_Q$  is taken equal to 10 in the absence of measurements for all the profiles considered in this study.

### Soil profiles, database, and site parameters

#### Overview of soil profiles

##### a. Set 1: Real Profiles (RP)

We consider three sets of soil profiles. The first one, termed RP, is composed of  $n_p = 858$  soil profiles. It was originally compiled by C. Cornou (Salameh 2016; Salameh et al. 2017) and consists of about 600 Japanese KiK-net sites, more than 200 sites from the USA, made available by D. Boore (<http://quake.usgs.gov/~boore>), and 22 European sites measured during the NERIES project (Di Giulio et al. 2012). The main characteristics of this set of site profiles are presented in Salameh (2016), Almakari et al. (2016) and Salameh et al. (2017): They are primarily usual (i.e., normally soft, with S-wave velocities generally  $>200$  m/s) and stiff soils, with shallow to intermediate thicknesses,  $<200$  m in most cases, with only few sites—about 50—with fundamental frequency below 1 Hz. They generally have “normally hard” to very hard underlying bedrock; the “bedrock” velocity, i.e., the velocity of the underlying half-space, varies from  $<500$  m/s to  $>3$  km/s.

Such variability in “bedrock” velocity is due to the velocity profile having been measured over a limited depth, not always reaching the underlying hard rock. Because part of the amplification is controlled by the velocity contrast, this variability may significantly bias the site response and assessment of the respective influence of the various site proxies considered here. It is usually considered within the earthquake engineering community that amplification should be measured with respect to a “standard rock” reference site with a velocity around 800 m/s. Consequently, the real soil profiles have been modified to have a normalized bedrock velocity of 800 m/s.

##### b. Set 2: Normalized profiles (NP):

The second data set is termed NP and is derived from the RP set using a homothetic transformation; all velocities are scaled by a factor of  $800/V_{\text{bedrock}}$  so that the

bedrock velocity is equal to 800 m/s for each profile in this “normalized profile” set, while the thickness of each layer is also scaled with the same factor to maintain an unchanged transfer function.

More specifically, for a site  $j$  with a bedrock velocity  $V_{\text{bedrock},j}$  the scaling is applied to the velocities and thicknesses of all layers  $i$  ( $i = 1, N_j$ ) as follows:

$$V'_{ij} = V_{ij} \cdot 800/V_{\text{bedrock},j} \quad (7)$$

$$h'_{ij} = h_{ij} \cdot 800/V_{\text{bedrock},j} \quad (8)$$

For real sites with very hard bedrock, e.g.,  $V_{\text{bedrock}} = 2500$  m/s, the scaled velocities may become unrealistically small at shallow depths; for instance, if  $V_1 = 120$  m/s, then, according to (7),  $V'_1 = 40$  m/s. Therefore, only normalized soil profiles with minimum scaled velocities exceeding 80 m/s are retained in this NP set, which reduces their number from 858 to 570.

##### c. Set 3: Truncated profile (TP)

The third set of soil profiles, termed TP, is derived simply by performing a “truncation” of each real soil profile; velocities are kept unchanged from surface until the depth  $Z_{800}$ , where the velocity first exceeds 800 m/s, and beyond this depth the velocity is set to 800 m/s. Whenever the bedrock velocity of the real soil profile is smaller than 800 m/s, the bedrock velocity is increased to 800 m/s. Therefore, this third TP set also consists of 858 soil profiles.

#### Site parameters

Each soil profile in each of the three sets can be partially described with a few site parameters, often called site proxies. In the present study, we investigate six of them, which have already been proposed by various authors in view of site classification (see, for instance, Castellaro et al. 2008; Cadet et al. 2012; Pitilakis et al. 2012, 2013), and provide information on the stiffness and/or thickness of soil columns. These parameters are the depth to bedrock (Depth); average shear velocity ( $V_{\text{sm}}$ ) over that depth, where subscript sm stands for mean value of the shear wave velocity; average shear wave velocity over the upper 30 m ( $V_{\text{s30}}$ ); shear wave velocity of bedrock ( $V_{\text{bedrock}}$ ); velocity contrast, i.e., ratio between shear wave velocities in bedrock and at the surface ( $C_v$ ); and soil profile fundamental frequency ( $f_0$ ). The exact definition of each of these six parameters is detailed below:

$$\text{Depth} = \sum_{i=1}^n h_i \quad (9)$$

Here, “bedrock” is the last known unit, which we consider as an underlying infinite half-space, while  $n$  is the number of layers above bedrock (see Fig. 2).

$$V_{sm} = \sum_{i=1}^n h_i / \sum_{i=1}^n \frac{h_i}{V_i} \tag{10}$$

where  $V_i = \sqrt{G_i/\rho_i}$  is the shear wave velocity in layer ( $i$ ).

$$V_{s30} = 30 / \sum_{i=1}^{l_{30}} \frac{h_i}{V_i} \tag{11}$$

where  $l_{30}$  is the number of distinct layers found in the top 30 m.

$$C_v = \frac{V_{Bedrock}}{V_1} \tag{12}$$

$f_0$  = fundamental soil frequency corresponding to the first peak (not necessarily the highest in amplitude) in the transfer function. In this study, for the sake of simplicity,  $f_0$  is determined using the Simplified Version of the Rayleigh Procedure (method # 7 in Dobry et al. 1976). Briefly, this approach is based on an approximation of the modal shape at the fundamental frequency, leading to the following Eqs. (13) and (14).

$$f_0 = \frac{\sqrt{\left(4 \left(\sum_{i=1}^n \frac{(z_i+z_{i+1})^2}{V_i^2} h_i\right) / \left(\sum_{i=1}^n (X_i + X_{i+1})^2 h_i\right)\right)}}{2\pi} \tag{13}$$

where  $(z_{i+1} + z_i)/2$  is the depth of midpoint of layer ( $i$ ) and  $X_i$  values correspond to the estimated fundamental mode shape at the top of each layer ( $i$ ), derived according to Dobry et al. (1976):

$$X_n = 0.; X_{i-1} = X_i + \frac{z_i + z_{i-1}}{V_i} h_i \tag{14}$$

**Distribution of site parameters**

The cumulative distributions of the log values of these six parameters are summarized in Fig. 3 for profile sets of RP, NP, and TP (more details can be found in Additional Files 1, 2, and 3, for each profile set, respectively). There is no distribution of  $V_{bedrock}$  for NP and TP sets, because it has a fixed value of 800 m/s. Most parameters follow a quasi-lognormal distribution, except for  $V_{bedrock}$ , which is significantly skewed with a mode at 3.2 km/s (Fig. 3 and Additional file 1), and is characterized by large variability.

Moreover, as these parameters are not fully independent, the coefficient of determination ( $R^2$ ) between each pair of parameters has been computed and is listed in Table 2 for the three RP, NP, and TP sets. There is an overall tendency for some correlation between velocity

parameters, especially  $V_{sm}$  and  $V_{s30}$ , but also the bedrock velocity  $V_{Bedrock}$  and  $V_{sm}$ ,  $V_{s30}$  and  $C_v$ , while much weaker correlations ( $R^2$  between 0.1 and 0.02) are observed for the parameter pairs  $(C_v, f_0)$ ,  $(Depth, V_{s30})$ ,  $(Depth, C_v)$  and  $(Depth, V_{Bedrock})$ . These correlation indicators are useful for selecting independent site parameters for the models relating site amplification to site characteristics.

**Computed amplification factors: main statistical characteristics**

**General background**

This section presents an overview of the computed sets of frequency-dependent AF, and their short- and mid-period average values (i.e., the Borchardt factors  $F_a$  and  $F_v$ ). This is essential as they constitute the learning set to identify the key parameters controlling the characteristics of site response.

AF values (Eq. 1) are calculated for the soil profiles RP, NP, and TP subjected to 14 seismic excitations. They may be written  $AF(P_k, \theta, S_l, T_i)$ , where:

- $P_k$ ,  $k = 1, \dots, n_p$  is introduced to identify the soil profile. Note that for RP and TP  $n_p = 858$  and for NP  $n_p = 570$  because we have imposed the minimal value of  $V_1$  as 80 m/s
- $\theta = 0$  for RP,  $\theta = 1$  for NP, and  $\theta = 2$  for TP.
- $S_l$ ,  $l = 1, 14$  is the  $l$ th excitation. Note that, as indicated below, the geometrical average of the 14 amplification factors has been computed for each site.
- $T_i$  ( $i = 1, \dots, 271$ ) is the  $i$ th structural period. AF values are systematically computed for 271 values, equally spaced between 0.01 and 10 s on a logarithmic period axis, i.e., also equally spaced between 0.1 and 100 Hz on a logarithmic frequency axis.

For instance,  $AF(P_{20}, 2, S_8, T_{55})$  stands for the AF obtained at the 50th period  $T_{55}$  for the truncated soil profile  $P_{20}$  subjected to seismic excitation  $S_8$ . After the AF is calculated for a particular profile  $k$ , and 14 seismic excitations, the site average amplification factor is computed as the geometrical average of the 14 individual amplification factors:

$$\log [AF_m(P_k, \theta, T_i)] = \left(\frac{1}{14}\right) \sum_{l=1}^{14} \log [AF(P_k, \theta, S_l, T_i)] \tag{15}$$

Hereafter, the abridged notation AF will stand for the average value  $AF_m(P_k, \theta, T_i)$ .

Simultaneously, for each profile  $P_k$ , AF variability derived from the 14 different time histories is quantified using the corresponding standard deviation:

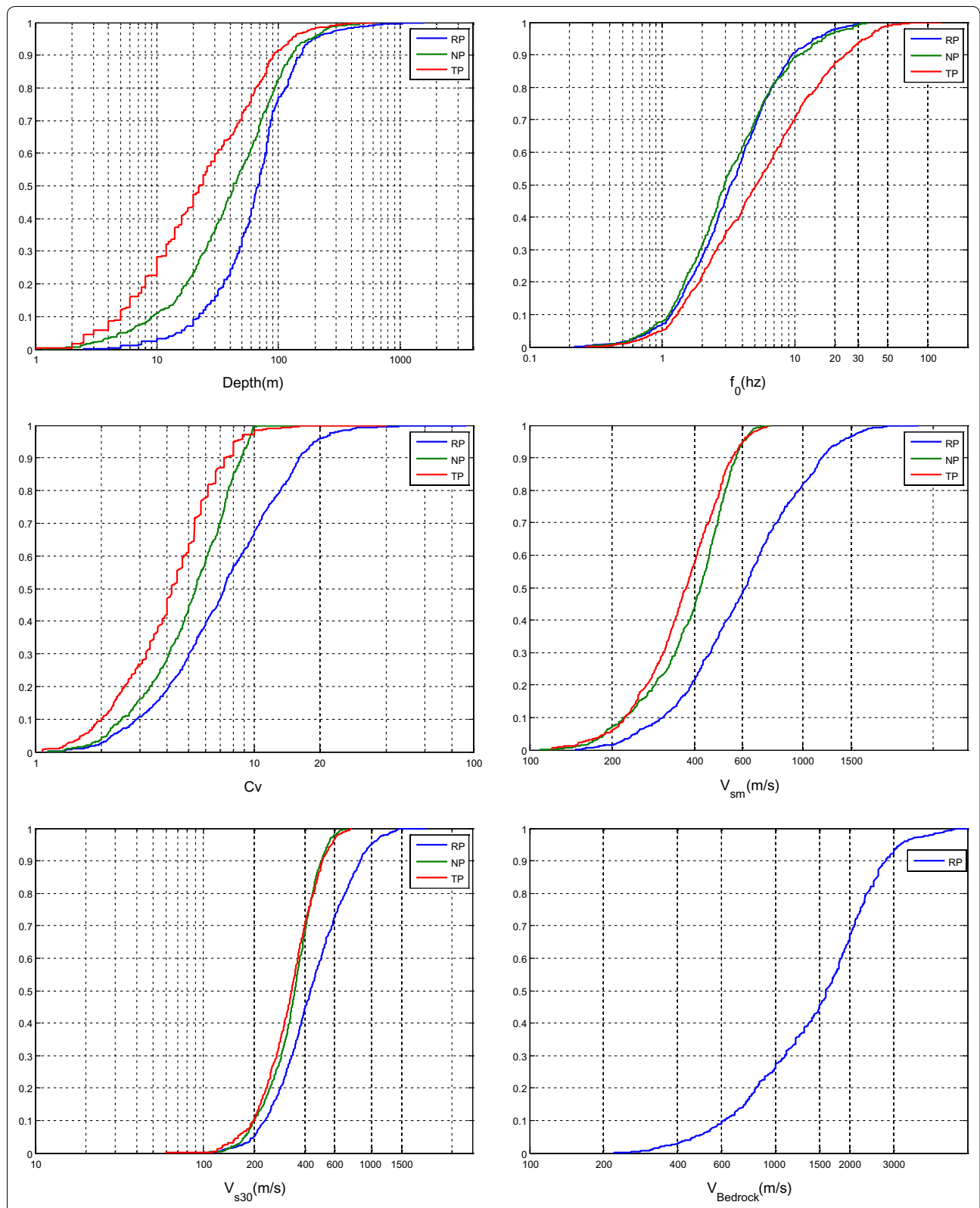


**Fig. 3** Cumulative distribution functions of the six selected site parameters for the soil profile sets of RP, NP, and TP; there are only five parameters for the two latter sets



**Table 2 Correlation between the various site parameters for the three profile sets (RP, NP, and TP, from top to bottom)**

RP						
RP	Depth	$f_0$	$C_v$	$V_{sm}$	$V_{s30}$	$V_{bedrock}$
Depth	1	0.3441	0.0903	0.2434	0.0388	0.0962
$f_0$		1	0.0196	0.1858	0.4050	0.3102
$C_v$			1	0.1596	0.0559	0.5345
$V_{sm}$				1	0.8515	0.6784
$V_{s30}$					1	0.5531
$V_{bedrock}$						1
NP						
NP	Depth	$f_0$	$C_v$	$V_{sm}$	$V_{s30}$	
Depth	1	0.4933	0.2137	0.4227		0.0299
$f_0$		1	0.0300	0.3680		0.1218
$C_v$			1	0.5297		0.5333
$V_{sm}$				1		0.8423
$V_{s30}$					1	1
TP						
TP	Depth	$f_0$	$C_v$	$V_{sm}$	$V_{s30}$	
Depth	1	0.4176	0.1973	0.2430		0.0664
$f_0$		1	0.3864	0.0629		0.2529
$C_v$			1	0.3852		0.5436
$V_{sm}$				1		0.8811
$V_{s30}$					1	1

The values in the cells correspond to the coefficient of determination  $R^2$  between the corresponding site parameters)

$$\sigma_{AF}(P_k, \theta, T_i) = \sqrt{\frac{\sum_{l=1}^{14} [\log(AF(P_k, \theta, S_l, T_i)) - \log(AF_m(P_k, \theta, T_i))]^2}{14}} \tag{16}$$

The  $\sigma_{AF}$  values are displayed in Fig. 4 for all 858 sites; they exhibit a significant frequency dependence, decreasing from  $\sim 0.1$  at short period to  $\sim 0.03$  at intermediate and long periods. These values are quite significant, especially at short periods; it would thus be meaningless to seek extremely precise models with residuals between observations and predictions much below these values.

A few additional parameters are introduced to measure the variability of the results.

- Average AF for all profiles, noted  $AF_0(\theta, T_i)$  and defined as the geometrical average of the  $n_p$  average AF ( $AF(P_k, \theta, T_i)$ ) noted for simplicity as  $AF_0$ :

$$\log(AF_0(\theta, T_i)) = \frac{1}{n_p} \sum_{k=1}^{n_p} [\log(AF_m(P_k, \theta, T_i))] \tag{17}$$

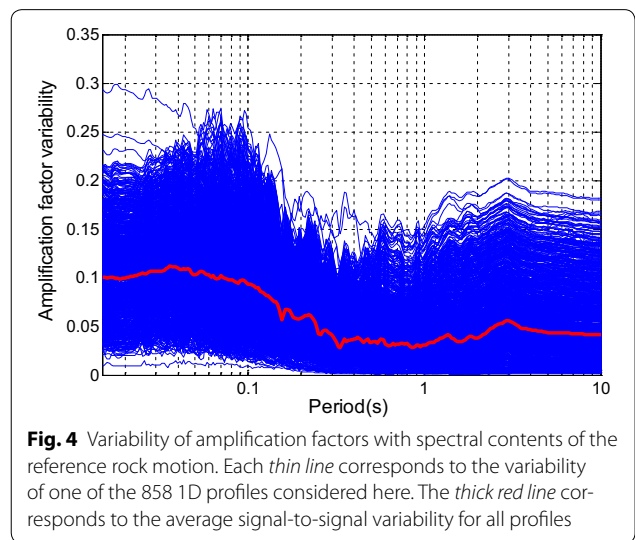


**Fig. 4** Variability of amplification factors with spectral contents of the reference rock motion. Each *thin line* corresponds to the variability of one of the 858 1D profiles considered here. The *thick red line* corresponds to the average signal-to-signal variability for all profiles

- Initial variability, defined as the initial standard deviation of the site average amplification factor over all profiles

$$\sigma_0(\theta, T_i) = \sqrt{\frac{1}{n_p} \sum_{k=1}^{n_p} [\log (AF_m(P_k, \theta, T_i)) - \log (AF_0(\theta, T_i))]^2} \quad (18)$$

- Maximum initial variability, defined as the peak value of the initial variability  $\sigma_0$  over the whole period range:

$$\sigma_{0max}(\theta) = \text{Max}_{T_i}[\sigma_0(\theta, T_i)] \quad (19)$$

- Overall initial variability, defined as the average over all periods of initial variability

$$\sigma_{0m}(\theta) = \frac{1}{n_T} \sum_{i=1}^{n_T} \sigma_0(\theta, T_i) \quad (20)$$

where  $n_T$  is the number of structural periods (or frequencies) used, i.e., 271.

### Means and variability of AF

For each profile set, we compute the  $n_p \times 14$  AF:  $AF(P_k, \theta, S_j, T_i)$ , the  $n_p$  average amplification factors  $AF_m$ :  $AF_m(P_k, \theta, T_i)$  together with their corresponding variability  $\sigma_{AF}(P_k, \theta, T_i)$ . We then derive the mean amplification factor  $AF_0(\theta, T_i)$  and associated initial variability  $\sigma_0(\theta, T_i)$ . The results are displayed in Fig. 5a, b, and c for each of the three RP, NP, and TP profile sets, respectively. The following observations are made.

- The peak period, i.e., the period with peak amplification, covers a broad range, from 0.08 s to about 3–4 s for the RP set, and from 0.1 s to about 1–2 s for the NP and TP sets.
- The corresponding peak amplification ranges from less than 1.5 up to 15. The highest peak (almost 15) is observed for RP, whereas for NP and TP the peak is less than 4.
- Some amplification factors exhibit a short-period de-amplification; a careful look at the corresponding profiles indicates it corresponds to profiles with low-velocity zones at some depth that act as a (weak) seismic isolator.
- The overall average amplification factor is close to 1 at long period (because long wavelengths do not “feel” the site structure over the first hundred meters), and it exhibits a very smooth and broad maximum with a value around 2 between 0.1 and 0.2 s. It is slightly below 2 at very short periods. It is significantly smaller than the peak values for individual profiles, which emphasizes the need to identify some relevant site parameters that may explain this site-to-site variability

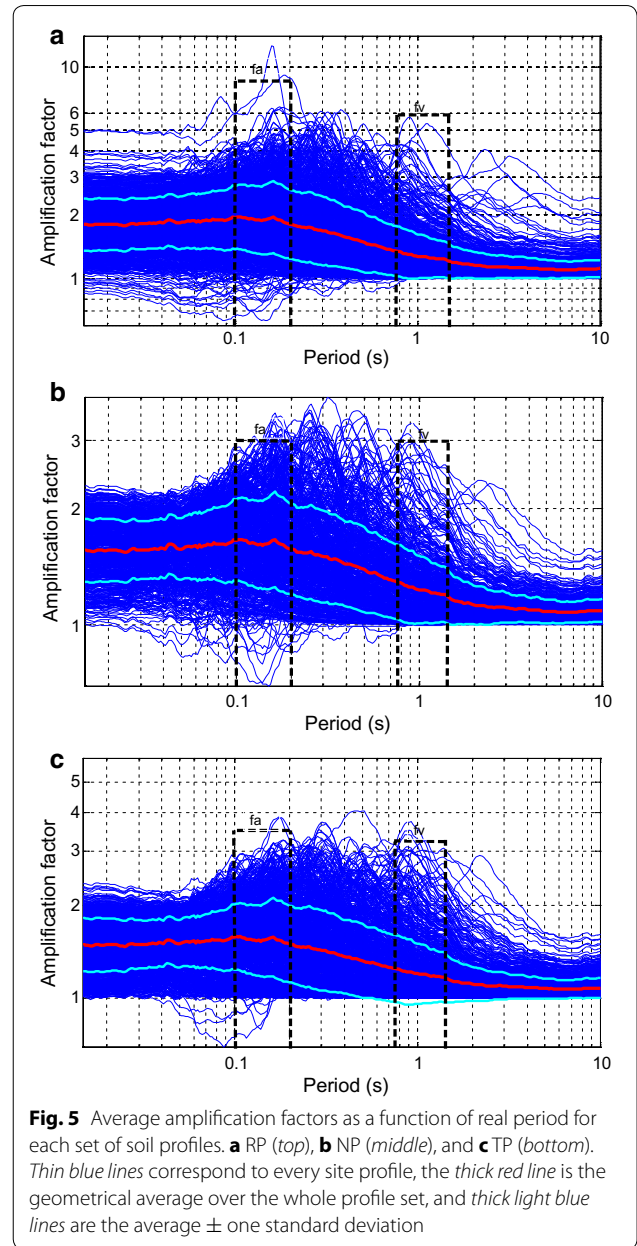


**Fig. 5** Average amplification factors as a function of real period for each set of soil profiles. **a** RP (top), **b** NP (middle), and **c** TP (bottom). Thin blue lines correspond to every site profile, the thick red line is the geometrical average over the whole profile set, and thick light blue lines are the average  $\pm$  one standard deviation

- The corresponding “initial variability”  $\sigma(\theta, T_i)$  is listed in Table 3 for RP, NP, and TP. It is maximum at intermediate periods (0.1–0.4 s, up to 45%) and minimum at long periods (around 10%).

### Means and variability of AF in the normalized frequency domain

As written in Eq. (15), AF can be described as a function of period  $T_i$ , i.e.,  $AF(P_k, \theta, T_i)$ , or alternatively frequency,  $f_i = 1/T_i$ . As indicated in Cadet et al. (2012), it may be helpful to normalize the frequency axis using the fundamental frequency of each site and compare all

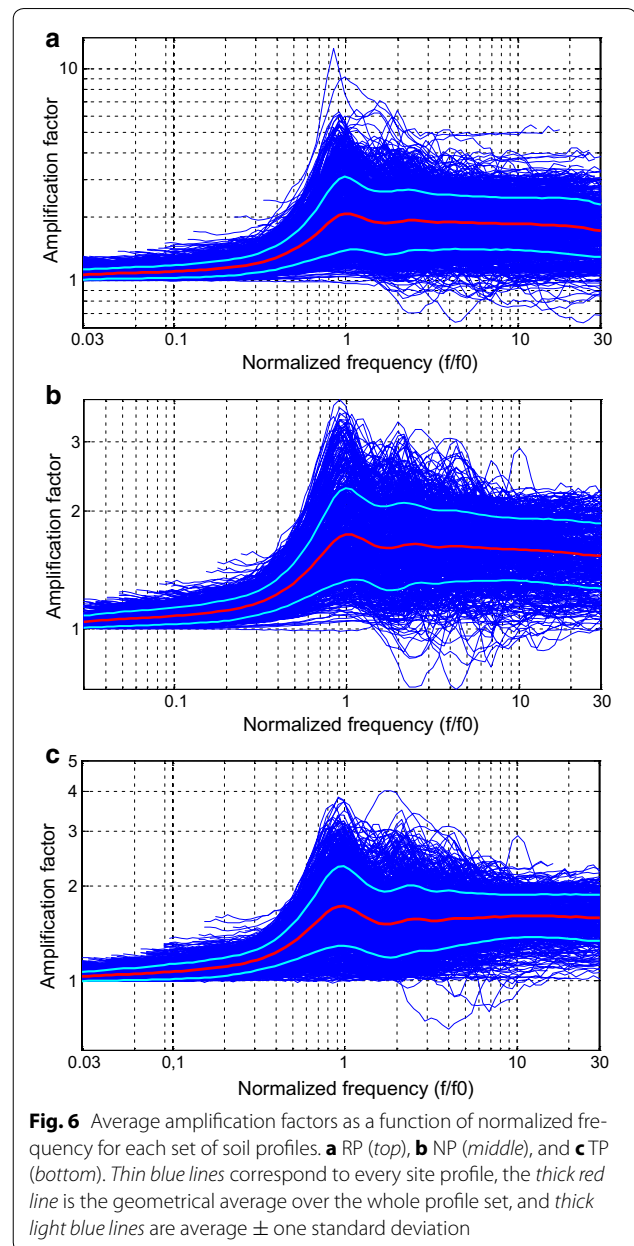
**Table 3 Initial variability values for the amplification factors in the real frequency domain for the RP, NP, and TP profile sets**

	RP-RF	NP-RF	TP-RF
Total initial variability $\sigma_{0m}$	0.1178	0.0846	0.0896
Maximum initial variability $\sigma_{0max}$	0.1717	0.1232	0.1317
$\sigma (T = 0.01 \text{ s})$	0.1227	0.0811	0.0866
$\sigma (T = 0.02 \text{ s})$	0.1226	0.0809	0.0861
$\sigma (T = 0.04 \text{ s})$	0.1206	0.0756	0.0759
$\sigma (T = 0.07 \text{ s})$	0.1314	0.0883	0.0861
$\sigma (T = 0.1 \text{ s})$	0.1494	0.1062	0.106
$\sigma (T = 0.2 \text{ s})$	0.1623	0.1169	0.1242
$\sigma (T = 0.4 \text{ s})$	0.1446	0.1089	0.1188
$\sigma (T = 0.7 \text{ s})$	0.1200	0.098	0.1093
$\sigma (T = 1.0 \text{ s})$	0.1040	0.0873	0.0982
$\sigma (T = 2.0 \text{ s})$	0.0626	0.0503	0.0552
$\sigma (T = 4.0 \text{ s})$	0.0477	0.033	0.036
$\sigma (T = 7.0 \text{ s})$	0.0388	0.027	0.0296
$\sigma (T = 10.0 \text{ s})$	0.0412	0.0297	0.0329

amplification factors as a function of the dimensionless normalized frequency  $\nu = f/f_0$ . Thus, AF can be rewritten as  $AF(P_k, \theta, \nu_i)$ , where  $\nu_i = f_i/f_0$ . The corresponding plots of all amplification factors, together with the average and average  $\pm$  one standard deviation, are displayed in Fig. 6a, b, and c for RP, NP, and TP sets, respectively.

As shown, the starting and ending abscissas of the  $AF(P_k, \theta, \nu_i)$  curves vary between profiles because of the variability in  $f_0$  values. For instance, for two profiles 1 and 2 with  $f_0$  values, respectively, 2 and 10 Hz, and an investigated “absolute frequency” range [ $f_{min} = 0.1 \text{ Hz}$ ,  $f_{max} = 100 \text{ Hz}$ ], the normalized frequency ranges [ $\nu_{min}$ ,  $\nu_{max}$ ] are, respectively, [0.05, 50] and [0.01, 10]. The number of available amplification factors thus varies with the normalized frequency  $\nu$ , as displayed in Fig. 7 for the three sets of profiles. All curves exhibit a clear plateau centered on  $\nu = 1$ , which systematically starts at  $\nu = 0.1$ , but ends at varying values depending on the profile set, around  $\nu = 10$  for RP and NP, and around  $\nu = 3$  for TP. Within this range of normalized frequency values, about 90% of the considered profiles provide amplification factor values. The corresponding average and variability, computed as indicated in Eqs. (15) to (20), have thus been calculated only for normalized frequencies ranging from 0.03 to 30, which corresponds to the availability of at least half the total number of profiles for each set (Fig. 7).

As shown in Fig. 6, the main consequences of this frequency normalization are to decrease the low-frequency scatter and slightly increase the mean AF values and associated scatter for  $\nu = 1$ , while the “high-frequency” mean values and standard deviations are comparable



to the short-period values shown in Fig. 5 and listed in Table 4. More explicitly, the widespread scatter of “real frequency” amplification factors, due to the combined variability of fundamental frequencies and amplification values, is redistributed in the normalized frequency domain. This transfers the variability primarily around and beyond the fundamental frequency.

**Focus on short and intermediate period (“Borcherdt factors”  $F_a$  and  $F_\nu$ )**

For a building code perspective, special attention is given to the short- and intermediate-period factors introduced

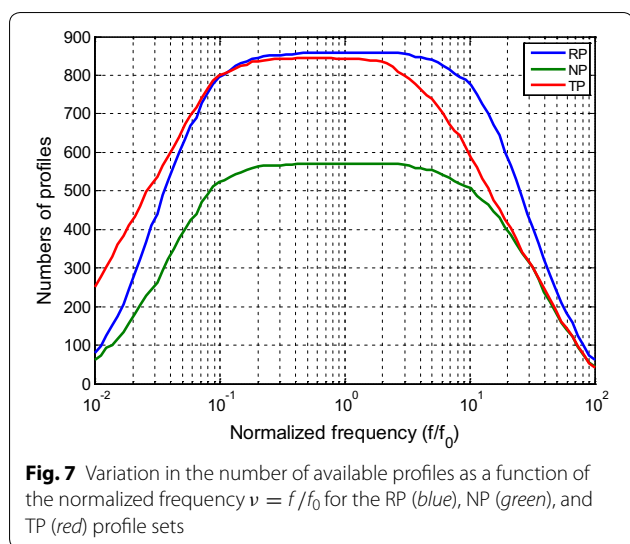


**Fig. 7** Variation in the number of available profiles as a function of the normalized frequency  $\nu = f/f_0$  for the RP (blue), NP (green), and TP (red) profile sets

**Table 4** Initial variability values for the amplification factors in the normalized frequency domain for the RP, NP, and TP profile sets

Data set	RP-NF	NP-NF	TP-NF
Total initial variability $\sigma_m$	0.1060	0.0724	0.0714
Maximum initial variability $\sigma_{max}$	0.1736	0.1187	0.1268
$\sigma (f/f_0 = 0.05)$	0.0261	0.0183	0.018
$\sigma (f/f_0 = 0.1)$	0.0301	0.0215	0.024
$\sigma (f/f_0 = 0.2)$	0.0373	0.0269	0.029
$\sigma (f/f_0 = 0.4)$	0.0600	0.0378	0.0418
$\sigma (f/f_0 = 0.7)$	0.1305	0.0904	0.1020
$\sigma (f/f_0 = 1.0)$	0.1673	0.1149	0.1228
$\sigma (f/f_0 = 2.0)$	0.1473	0.1101	0.1074
$\sigma (f/f_0 = 4.0)$	0.1281	0.0912	0.0908
$\sigma (f/f_0 = 7.0)$	0.1248	0.0829	0.0741
$\sigma (f/f_0 = 10.0)$	0.1239	0.0794	0.0682
$\sigma (f/f_0 = 20.0)$	0.1312	0.0833	0.0712

by Borchardt (1994, 2002) to specify the short-period level (acceleration plateau) and intermediate-period level (velocity response). In the absence of any consensual, widely accepted definition, we defined them as follows:

- $F_a$  is taken as the geometrical mean of AF for periods in the range [0.1 s, 0.2 s]
- $F_v$  is taken as the geometrical mean of AF for periods in the range [0.75 s, 1.5 s]

The corresponding period ranges are displayed in Fig. 5. Considering that the amplification factors were derived for equally spaced values on a logarithmic period axis, these two average values thus correspond to exactly the same number of points.

### Resulting sets of AF and Borchardt factors

The methodology detailed in this section leads to three sets of amplification factors AF for RP, NP, and TP, which can be described as a function of real or normalized frequency. The three real frequency sets have also been summarized with the two Borchardt factors, because these scalar values corresponding to the short and intermediate periods are widely used to translate the impact of site effects in building codes. The main issue now is to understand the influence of site parameters on shaping the values of both the AF and Borchardt factors. To reach this goal, we use the generalized regression neural network (GRNN) approach, described in the next section.

### Description of the neural network approach

#### Scope and principles of artificial neural networks

In general, the scope of the artificial neural network approach is to establish relationships, or classifications, between a set of output parameters and set of input parameters, which are too complex to be “guessed” using simple functional forms. It is based on a “learning phase,” where a large number of “known points,” with known input and output values, are used to train the neural network system in an “optimal” way, so that it can be later used to predict (unknown) output values for a new set of input values, that should fall in the domain of the hyperspace that is properly sampled by the learning data set. The flexibility of neural networks has fostered their use in many different disciplines for regression and classification purposes, where they have proven very powerful. For instance, in engineering seismology, they have been applied to site amplification issues (Giacinto et al. 1997; Paolucci et al. 2000), establishing GMPEs (see Derras et al. 2012 for a review of previous applications, and Derras et al. 2014, 2016 for recent developments), and generating spectrum compatible time histories (Ghaboussi and Lin 1998; Lin and Ghaboussi 2001).

The objective of an ANN is to mimicking human brain behavior with interconnecting artificial neurons between input and output layers that contain input and output data, with very often hidden layers in between. Each neuron is a kind of microprocessor that connects two layers  $l$  and  $l + 1$  through accepting a set of inputs from layer  $l$ , performing a weighted sum of all these inputs, and processing this weighted sum through an “activation function,” which may be linear or nonlinear, and essentially makes this neuron “fire” when the input weighted sum is large enough.

The main degrees of freedom of an ANN, in addition to its architecture (number of hidden layers, and number of neurons in each of them), are the weights for each neuron (together with another parameter named the “bias,” see Derras et al. 2012) and shape of the activation function.

The learning from the data set is stored in the weights and bias through some regression process that accounts for the distance between actual output data and predicted values. The architecture and selection of activation functions are the responsibility and “art” of the user.

In short, two main types of architecture, which are associated with two main types of summations and activation functions, exist. The multi-layer perceptron (MLP) architecture first performs distinct linear combinations of input variables that feed each hidden neuron, which then processes it with its specific “activation function” (linear ramp, threshold—“Heaviside” like, sigmoid, hyperbolic tangent, etc.). The outputs are then recombined in a similar way between the hidden and output layers. The convergence scheme consists of back-propagating the error, i.e., distance between predictions and observations, to tune the weights and bias terms corresponding to each neural connection and minimize the overall error. Radial basis function (RBF) architecture starts with computing the “distances” between a given input value and representative set of all the input data used for the training/learning phase and then predicts the corresponding output after “interpolating” the known output values on the basis of those distances. Additional details are given in Sect. 4.2.

#### The special case of generalized regression neural network (GRNN)

Specht (1991) proposed a method that he called “generalized regression neural network” (GRNN), because it uses the artificial neural network approach to perform general linear or nonlinear regressions. The general idea is to extend classical regressions based on a priori functional forms to an approach where no functional form is needed. GRNN draws the estimates directly from the “proximity” (distance) to training data. It is thus a special kind of radial basis neural networks (Cigizoglu and Alp 2005; Kim et al. 2004), where the “distance”  $d_j$  to each data point in the training set  $X_j$  is used to estimate the relative weight  $w_j$  of the corresponding output  $Y_j$  through a “kernel” function having a bell shape (here, a Gaussian function  $\exp(-b^2(d_j)^2)$ ). For vectorial inputs (here we use up to six site parameters), the “distance” term  $d_j$  for a given profile is considered the Euclidian distance derived from the considered site parameters, as detailed as follows.

The GRNN approach can thus be seen either as a relatively straightforward interpolation algorithm, a “kernel-based” approximation method, or as a special kind of neural network. We will start with presenting the simple equations corresponding to the former and then briefly explain its implementation in the general framework of neural networks.

Let  $(X_j, Y_j)$  with  $j = 1, Q$  be the sample data set;  $X_i$  is a vector with  $R$  components, which are here the site parameters (up to six) for each soil profile considered in either data set (RP, NP, or TP), and  $Y_i$  is a scalar equal to the corresponding amplification factor at a given frequency (or  $F_a$  or  $F_v$ ).

Let now  $\mathbf{x}$  be a vector containing the same  $R$  site parameters, corresponding to a new soil profile, which has not been considered in the initial data set (RP, NP, or TP). The goal is to predict the corresponding amplification factor  $y$ . This is achieved with the following formula:

$$y = \sum_{j=1}^Q Y_j w_j / \sum_{j=1}^Q w_j \quad (21)$$

with  $w_j$  being the weights of each training data, estimated from their Euclidian distance to the point of interest

$$w_j = e^{-[b \text{dist}(\bar{\mathbf{x}}, \bar{X}_j)]^2} \quad (22)$$

with:

$$\text{dist}(\bar{\mathbf{x}}, \bar{X}_j) = \bar{x} - \bar{X}_j = \sqrt{2 \sum_{k=1}^R (x_k - X_{jk})^2} \quad (23)$$

The output  $y$  is thus simply estimated as a weighted average of the amplification factors of the training set, with the weighting derived from the distance between the considered site and site proxies from the training set; thereby, nearby sites contribute most heavily to the estimate. The only “free” parameter in this approach is the “ $b$ ” value, which controls the width of the Gaussian function used for assigning interpolation weights  $w_j$ . Larger  $b$  values result in sharper bell-shape functions around each point of the training data set.

The topology of a GRNN, as described in Fig. 8, consists of four layers, with two hidden layers between the classical input and output layers: the first hidden layer is called the “pattern layer,” the second is the “summation” layer, which is explained as follows.

- The input layer simply consists of the values of the selected site parameters (up to six in the present case)
- The next “pattern” layer computes the weights  $w_j$  from the distance of the considered site parameters to each site used in the training set (Eq. 23). The number of neurons in this layer,  $Q$ , is equal to the number of data in the training set (here, up to 858). The function deriving the weights  $w_j$  from the distance to each data point  $j$  is called a “radial basis function” and has a bell shape centered at 0 distance. As mentioned previously, here we used a Gaussian



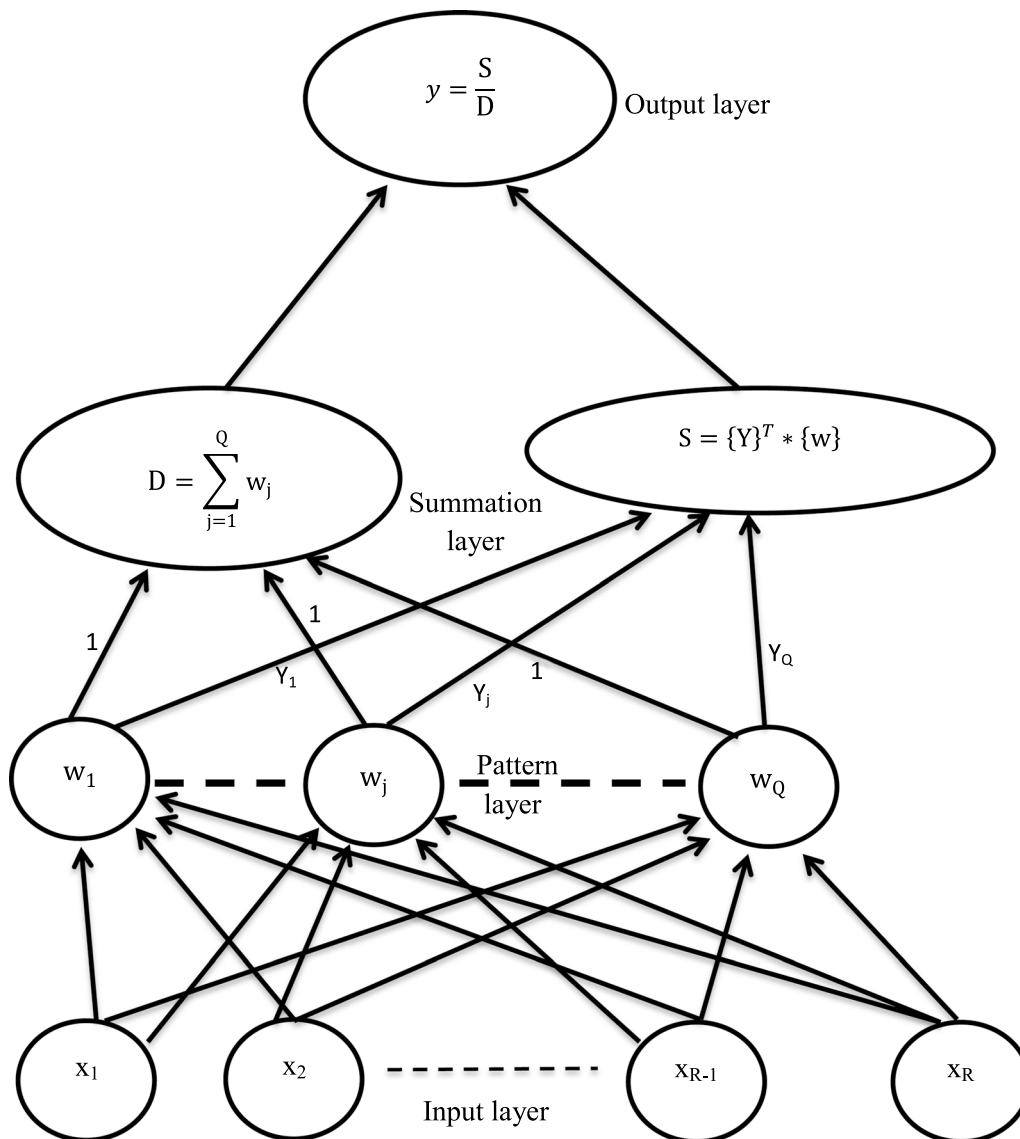


**Fig. 8** General architecture of a neural network in the GRNN approach. Four layers are displayed from *bottom* (input layer: site proxies) to *top* (output layer: predicted amplification factor)

RBF characterized by a width parameter  $b$ . In the neural network language, it is often called a “bias” (Wasserman 1993).

- The third layer is the second hidden layer and is called the “summation layer.” It combines the distance-based weights computed in the previous layer to perform the summation required to estimate the output. It consists of two neurons, related to the  $Q$  neurons of the previous layer, which, respectively, perform two different summations,  $S = \sum_{j=1}^Q Y_j w_j$  and  $D = \sum_{j=1}^Q w_j$ . In the neural network framework,

the weights  $w_j$  are seen here as the outputs of the previous layer, and the training set outputs  $Y_j$  as the weights of the summation achieved by the first neuron.

- Finally, the output layer consists of one single neuron simply performing the division of  $S$  by  $D$ .

More detailed information about GRNN can be found in Specht (1991), Wasserman (1993), Kim et al. (2004), Cigizoglu and Alp (2005) or Hannan et al. (2010).

### Present implementation

For the present application, the implementation is separately completed on the three profile sets of RP, NP, and TP. These databases are described in Sect. 2.4.1. The initial set of data to feed the neural network is constituted of  $n_P$  profiles and their corresponding amplification factors (i.e.,  $AF_m(P_k, \theta, T_i)$  or  $AF_m(P_k, \theta, \nu_i)$ ). The input vector consists of a subset of the six site parameters for the RP set, and five site parameters for the NP and TP sets, for which the bedrock velocity is constant. The output consists of the calculated AF values for a given period or normalized frequency (271 values), and the Borchardt factors  $F_a$  and  $F_v$ . This output is labeled  $AF_{GRNN}(P_k, \theta, T_i)$  and depends on the number of site proxies used. There is one GRNN model for each scalar output, i.e., 271 scalar models for each period  $T_i$  of  $AF_m(P_k, \theta, T_i)$ , 271 scalar models for each normalized frequency  $\nu_i$  of  $AF_m(P_k, \theta, \nu_i)$ , one for  $F_a$  and one for  $F_v$ . All sets of 544 GRNN models are labeled hereafter as xP-yF, according to the corresponding profile set (RP, NP, or TP) and the type of frequency values (real or normalized), for instance, RP–RF for real profiles and real frequencies, TP–NF for truncated profiles and normalized frequencies. All possible combinations of input site parameters were considered, so that, as listed in Table 5, 186 sets of GRNN models are obtained: 63 for RP–RF (all possible combinations within six site parameters), 31 for RP–NF, NP–RF, and TP–RF (all possible combinations within five site parameters), and 15 for RP–NF and TP–NF (all possible combinations within four site parameters).

In each case, the networks are trained by dividing the data set into a training set (75%) and a testing set (25%), the elements of which are randomly swapped from one set to another until the width of the Gaussian is robustly

estimated. The Gaussian width is the only free parameter optimized. The full data set is then used to estimate the performance of the GRNN model using various non-independent indicators, such as the coefficient of correlation, standard deviation of residuals, and reduction in variance with respect to the initial variability.

## Results

### Comparisons between original AF and GRNN predictions

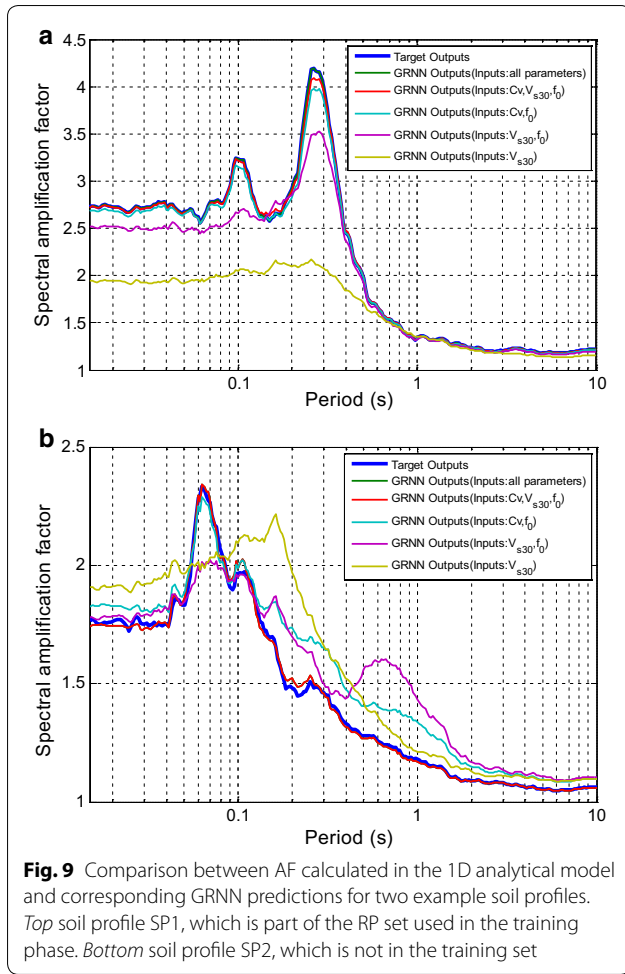
Our first goal is to test the ability of the GRNN models using only a limited number of site parameters to satisfactorily predict AF values. To achieve that goal, we derived a large number of GRNN models using all possible combinations of input parameters and analyzed their respective performance by comparing the level of the standard deviation of residuals (predicted – actual values) to the initial variability values for each period, i.e.,  $\sigma_0(\theta, T_i)$ , and to the overall variability  $\sigma_{0m}(\theta)$  as previously defined.

Before discussing these performances, we provide in Fig. 9 an example comparison between AF predicted with a few GRNN models to actual AF (computed from the full 1D soil column, as described in Sect. 3) for two soil profiles SP1 and SP2 (see Table 6). These soil profiles have been selected arbitrarily: SP1 is part of the initial RP profile set, SP2 is not. The corresponding site proxies, as also listed in the same Table 6, fall within the “core” of the initial data set (see Fig. 3 and Additional Files 1, 2, and 3).

As shown in Fig. 9a for soil profile SP1 and Fig. 9b for soil profile SP2, the predicted AF values are clearly different from the actual ones, especially when only a small number of site proxies are considered. The differences between predictions and actual amplification factors vary between soil profiles. This difference indicates the

**Table 5** List of considered GRNN models

Output values	Period/normalized frequency	Set of profiles	Set of explanatory variables (site parameters)	Combinations
$AF(T), F_a, F_v$	Period	RP	6: Depth, $f_{0r}$ , $C_v$ , $V_{smr}$ , $V_{s30r}$ , $V_{bedrock}$	63 = 6 1-parameter, 15 pairs, 20 triplets, 15 quadruplets, 6 quintuplets, 1 (all 6 parameters)
$AF(f/f_0)$	Normalized $f/f_0$	RP	5: Depth, $C_v$ , $V_{smr}$ , $V_{s30r}$ , $V_{bedrock}$	31 = 5 1-parameter, 10 pairs, 10 triplets, 5 quadruplets 1 (all 5 parameters)
$AF(T), F_a, F_v$	Period	NP	5: Depth, $f_{0r}$ , $C_v$ , $V_{smr}$ , $V_{s30}$	31 = 5 1-parameter, 10 pairs, 10 triplets, 5 quadruplets 1 (all 5 parameters)
$AF(f/f_0)$	Normalized $f/f_0$	NP	4: Depth, $C_v$ , $V_{smr}$ , $V_{s30}$	15 = 4 1-parameter, 6 pairs, 4 triplets, 1 (all 4 parameters)
$AF(T), F_a, F_v$	Period	TP	5: Depth, $f_{0r}$ , $C_v$ , $V_{smr}$ , $V_{s30}$	31 = 5 1-parameter, 10 pairs, 10 triplets, 5 quadruplets 1 (all 5 parameters)
$AF(f/f_0)$	Normalized $f/f_0$	TP	4: Depth, $C_v$ , $V_{smr}$ , $V_{s30}$	15 = 4 1-parameter, 6 pairs, 4 triplets, 1 (all 4 parameters)



importance of analyzing the standard deviation of residuals to obtain a statistically meaningful insight into the relative performances of each considered site proxy in controlling the AF.

### Analysis of the prediction residuals

The error between prediction and actual values (Eqs. 24–26) is estimated and compared with the initial variabilities (Eqs. 18–20).

- For each period and each GRNN model, a period-dependent error term representing the standard deviation of residuals is computed as follows for comparison with the initial variability term  $\sigma_0(\theta, T_i)$  (Eq. 18):

$$\begin{aligned} \varepsilon_{\text{GRNN}}(\theta, T_i) &= \sqrt{\frac{1}{n_p} \sum_{k=1}^{n_p} [\log(\text{AF}_{\text{GRNN}}(P_k, \theta, T_i)) - \log(\text{AF}_m(P_k, \theta, T_i))]^2} \end{aligned} \quad (24)$$

- Similarly, in relation to the maximum initial variability  $\sigma_{0\text{max}}(\theta)$  (see Eq. 19), a “maximum error” is defined as the maximum over all periods/frequencies of  $\varepsilon_{\text{GRNN}}(\theta, T_i)$ :

$$\varepsilon_{\text{GRNN,max}}(\theta) = \text{Max}_{T_i}[\varepsilon_{\text{GRNN}}(\theta, T_i)] \quad (25)$$

- Finally, similar to the overall initial variability term  $\sigma_{0m}(\theta)$  (see Eq. 20), an overall error is defined as the average over all periods of the error term:

$$\varepsilon_{\text{GRNN,m}}(\theta) = \frac{1}{n_T} \sum_{i=1}^{n_T} \varepsilon_{\text{GRNN}}(\theta, T_i) \quad (26)$$

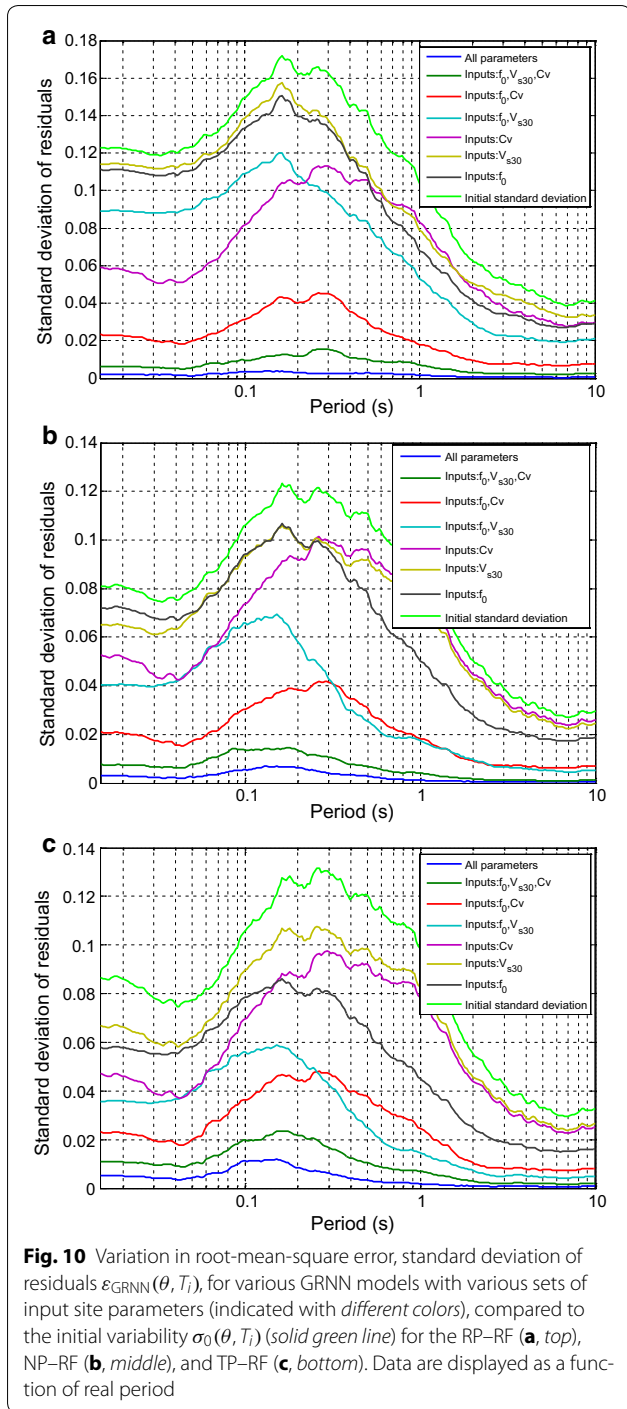
Examples of the period-dependent error term  $\varepsilon_{\text{GRNN}}(\theta, T_i)$  are displayed in Figs. 10, 11 for the real period and normalized frequency domains, respectively, together with the initial variabilities,  $\sigma(\theta, T_i)$ , of the amplification factor sets. In the former case, the few considered GRNN models are the same as those considered for Fig. 9, i.e., the pairs  $(C_v, f_0)$  and  $(f_0, V_{S30})$ , triplet

**Table 6** Velocity profile and site parameters for the two example soil profiles SP1 (part of the RP set) and SP2 (outside RP set)

Layer #	Soil profile 1		Soil profile 2	
	Thickness $h_i$ (m)	S-wave velocity $V_i$ (m/s)	Thickness $h_i$ (m)	S-wave velocity $V_i$ (m/s)
1	4	150	2	120
2	10	260	14	510
3	6	420	39	720
4	12	950	108	900
5	40	1470	Bedrock	1000
6	Bedrock	1850		

Soil profile	Depth (m)	$f_0$ (Hz)	$V_{sm}$ (m/s)	$C_v$	$V_{s30}$ (m/s)	$V_{\text{bedrock}}$ (m/s)
SP1	72	3.69	603	12.33	333	1850
SP2	163	1.44	746	8.33	472	1000

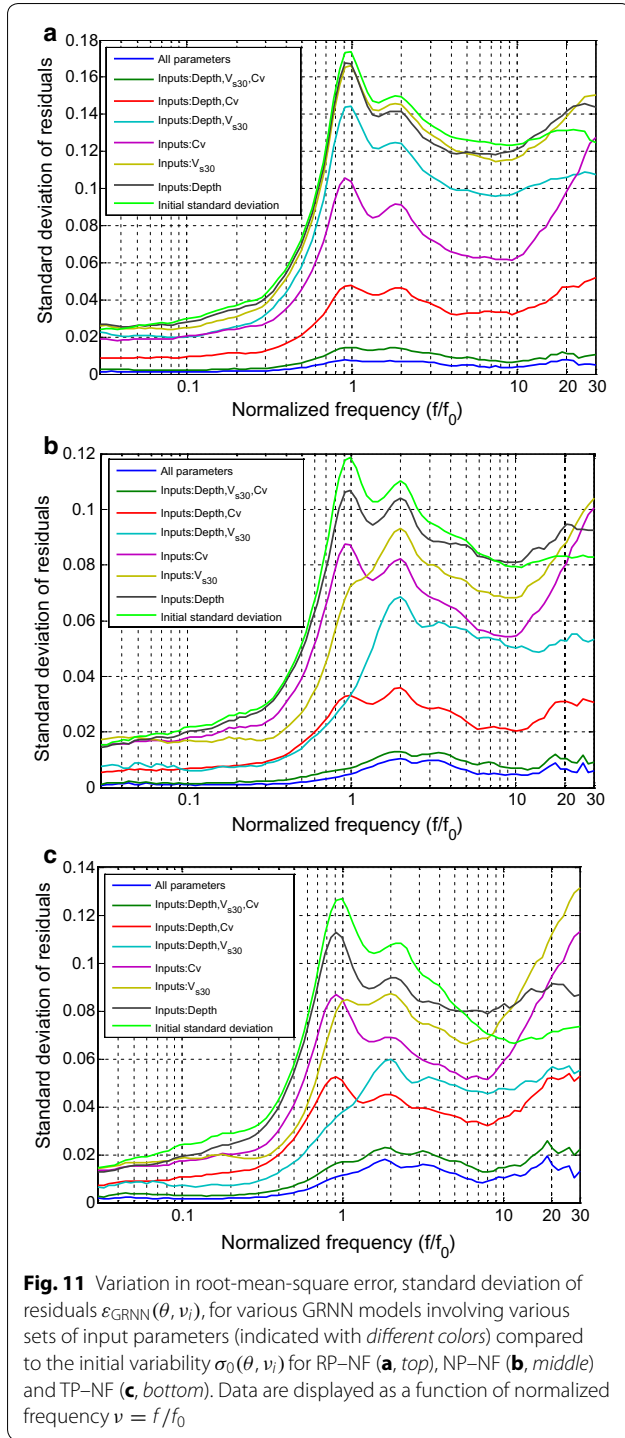


( $C_v, f_0, V_{S30}$ ), and “all parameter” case, plus three cases of one parameter GRNN, considering individual site proxies  $C_v, V_{S30}$  and  $f_0$ . In the normalized frequency domain case, the parameter “ $f_0$ ” is replaced with the parameter “Depth,” which is fully independent from the velocity parameters. Figures 10 and 11 exhibit several noticeable features:

- $C_v$  alone allows a significant explanation of the AF, i.e.,  $\varepsilon(\theta, T_i)$  is significantly smaller than  $\sigma_0(\theta, T_i)$ . It performs even better at short periods than when considering two other site proxies, such as ( $f_0, V_{S30}$ ) (Fig. 11a). The latter result, however, is not valid for profile sets NP and TP, because of the uniformity of bedrock velocity, which lowers the relative importance of  $C_v$  compared to  $V_{S30}$ .
- The three-parameter GRNN model, based on ( $C_v, f_0, V_{S30}$ ), is very powerful to predict actual AF, with residual errors less than 15% of the initial variability. Notably, the “all parameter” GRNN models using “only” five to six parameters provide very satisfactory predictions, with residual errors  $\varepsilon(\theta, T_i)$  less than 5% of the initial variability.
- The largest root-mean-square errors are systematically found in the short- to intermediate-period range for the real period domain (Fig. 10) and around the fundamental frequency  $f_0$  for the normalized frequency domain (Fig. 11). This actually corresponds to the frequency range of the largest initial variability.
- The widely used  $V_{S30}$  parameter is found to have a notably good performance only when associated with the fundamental frequency and when bedrock velocity is uniform (Fig. 11b, c). For all other cases (Fig. 10), it performs significantly worse than the single parameters  $C_v$  or  $f_0$ .

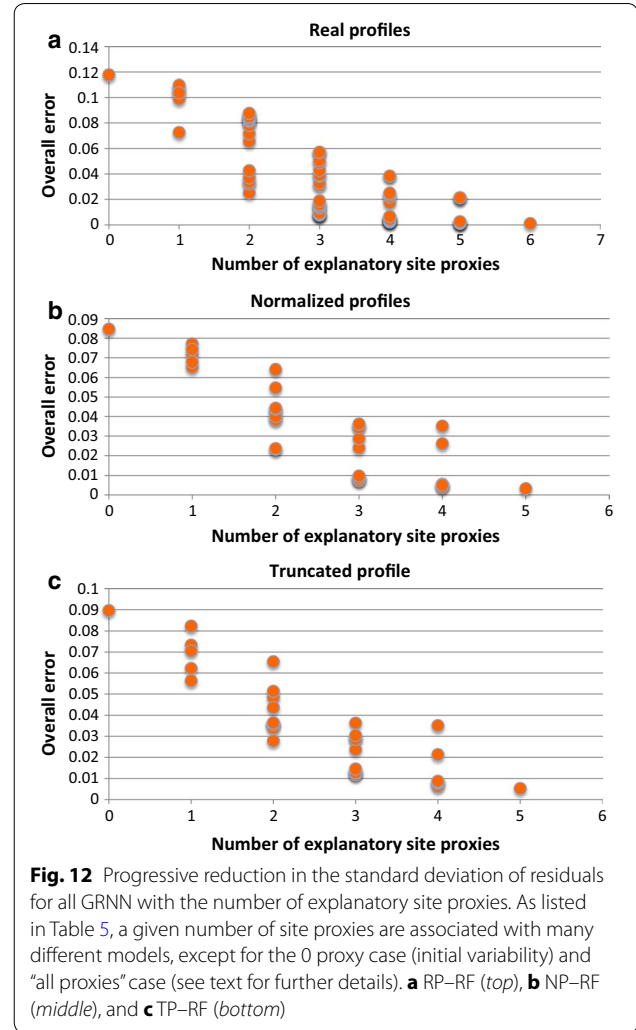
These results are only partial as only seven of the many possible models (for instance, up to 63 for the RP–RF case, see Table 5) are considered. Figure 12 displays the evolution of overall error  $\varepsilon_m(\theta)$  with the number of proxies for all combinations of site proxies. As listed in Table 5, a given number of explanatory site proxies are associated with many different models. For example, for the RP–RF case, there are 15 possible combinations involving pairs of proxies, 20 involving triplets, and 15 involving quadruplets of site proxies. The zero-proxy value of  $\varepsilon_m(\theta)$  corresponds to the initial variability  $\sigma_{0m}(\theta)$ . While it clearly decreases with an increasing number of explanatory site proxies, it also exhibits a significant scatter for a given number of proxies. This indicates that some site proxies perform better than others in controlling the amplification factor.

Considering the large number of possible combinations (indicated in Table 5), we analyzed the respective performances of each proxy by evaluating, for a given number of site proxies, the average value of  $\varepsilon_m(\theta)$  for all the proxy combinations that involve the considered proxy. For instance, in the RP–RF case, there are 15 possible combinations of pairs of site proxies. Within all these pairs, we characterize the performance of a given proxy (for instance,  $V_{S30}$ ) using the average value  $\varepsilon_m(\theta)$  for the five combinations involving that proxy, i.e., the five pairs



$(V_{S30}, C_v)$ ,  $(V_{S30}, V_{\text{bedrock}})$ ,  $(V_{S30}, f_0)$ ,  $(V_{S30}, \text{Depth})$  and  $(V_{S30}, V_{S_m})$ . This allows us the possibility of identifying the importance of each site proxy using the following quantity:

$$\text{RS}_m(\theta) = 1 - \frac{\overline{\varepsilon_m(\theta)}}{\sigma_m(\theta)} \quad (27)$$



where  $\text{RS}_m(\theta)$  is the reduction in standard deviation.

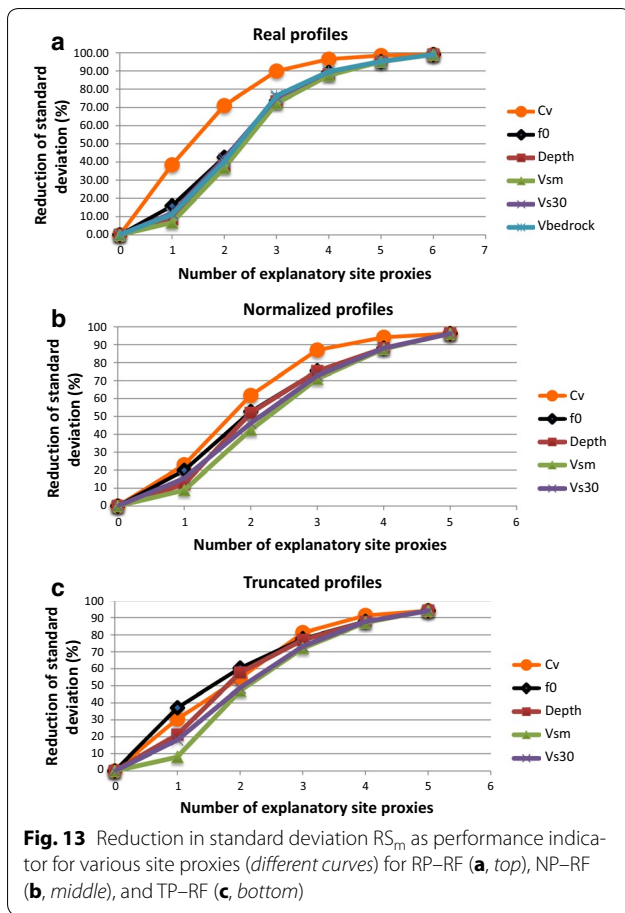
Another way to measure the importance of each site proxy is the reduction in variance:

$$\text{RV}_m(\theta) = 1 - \frac{(\varepsilon_m(\theta))^2}{(\sigma_m(\theta))^2} = \text{RS}_m(\theta)(2 - \text{RS}_m(\theta)) \quad (28)$$

The procedure is repeated for all the possible number of site proxies, which culminates in the curves displayed in Fig. 13 for the three RP, NP, and TP sets. Similar results are obtained for the normalized frequency domain and are provided as additional files.

For the RP and NP sets, one parameter systematically performs better than the others to explain the amplification factor, the velocity contrast  $C_v$  (Fig. 13a). This result is not valid for the TP set (Fig. 13c), for which  $f_0$  outperforms the other proxies as long as only one or two explanatory site proxies are considered.





Such results are easily understandable, as the velocity contrast does dominate the impedance contrast that in turn controls the actual amplification for the simple, single-layer case. All other parameters perform similarly, however, with a slightly better performance for the fundamental frequency and a slightly worse one for the “whole thickness” parameters Depth and  $V_{sm}$ . As for the widely used  $V_{S30}$  proxy, it performs better than “Depth” and “ $V_{sm}$ ” but worse than  $C_v$ ,  $f_0$ , and  $V_{bedrock}$  for the RP case, and it is one of the two worst proxies (with  $V_{sm}$ ) for the

NP and TP sets. Notably, the Depth proxy performs satisfactorily only for constant velocity bedrock.

Therefore, it would be desirable to measure the velocity contrast between bedrock and surface for any site where possible. Unfortunately, such measurements are challenging and/or expensive, and this “optimal” site proxy is almost never available. Therefore, what is the optimal “second choice”? When  $C_v$  is not available, it is most often because  $V_{bedrock}$  could not be measured. A careful look at Table 7 indicates that the pair  $(V_{S30}, f_0)$  provides prediction errors similar to  $C_v$  alone and that the next relatively efficient site parameter to be considered in combination with others is “Depth.”

Another interesting result is the potential usefulness of considering the normalized frequency space to predict the amplification factor from a few site proxies. A comparison between the performances of real and normalized frequency GRNN models (Fig. 13 and Additional File 4, respectively) clearly indicates that  $RS_m(\theta)$  is reduced slightly more when considering  $f_0$  directly as an input parameter, rather than simply for normalizing the frequency axis. For instance,  $RS_m(1)$  is 79% with the parameter pair  $(C_v, f_0)$  and 93% for the parameter triplet  $(C_v, f_0, V_{S30})$  for the RP–RF case, while it is only 38% with the parameter  $(C_v)$  and 68% for the parameter pair  $(C_v, V_{S30})$  for the RP–NF case (see Table 7). The gain in simplicity of the normalized frequency approach, which provides less complex prediction formulae with one fewer parameter, is balanced by a significantly poorer performance.

**Variation in Borchardt factors using GRNN**

As indicated previously, site effects can be simply characterized with the two Borchardt factors,  $F_a$  and  $F_v$ , especially from a regulatory perspective. Therefore, we compute the Borchardt factors for the GRNN model based the pair of site proxies  $(f_0, V_{S30})$ , which proves to be fairly efficient. Figures 14 and 15 display the dependence of these two factors as a function of  $V_{S30}$  and  $f_0$ . For all cases, this dependence is considered within the 5–95%

**Table 7** Standard deviation of model residuals for various GRNN models implying the initial, actual frequency amplification factors (RP, NP, TP cases, last three columns) for various combinations of site parameters

Number of parameters	Considered site parameters	Error (RP)	Error (NP)	Error (TP)
All (6)	Depth + $f_0$ + $V_{sm}$ + $C_v$ + $V_{S30}$ + $V_{bedrock}$	0.0011	0.0032	0.0053
3 (best triplet)	$f_0$ + $C_v$ + $V_{S30}$	0.0079	0.0079	0.0118
2 (best pair)	$f_0$ + $C_v$	0.0251	0.0233	0.0278
2 (convenient pair)	$f_0$ + $V_{S30}$	0.0782	0.0382	0.0339
1 (best)	$C_v$	0.0725	0.0652	0.0622
1 (usual)	$V_{S30}$	0.1038	0.0715	0.0733
1	$f_0$	0.099	0.0678	0.0563
Overall initial variability term $\sigma_m(\theta)$		0.1178	0.0846	0.0896

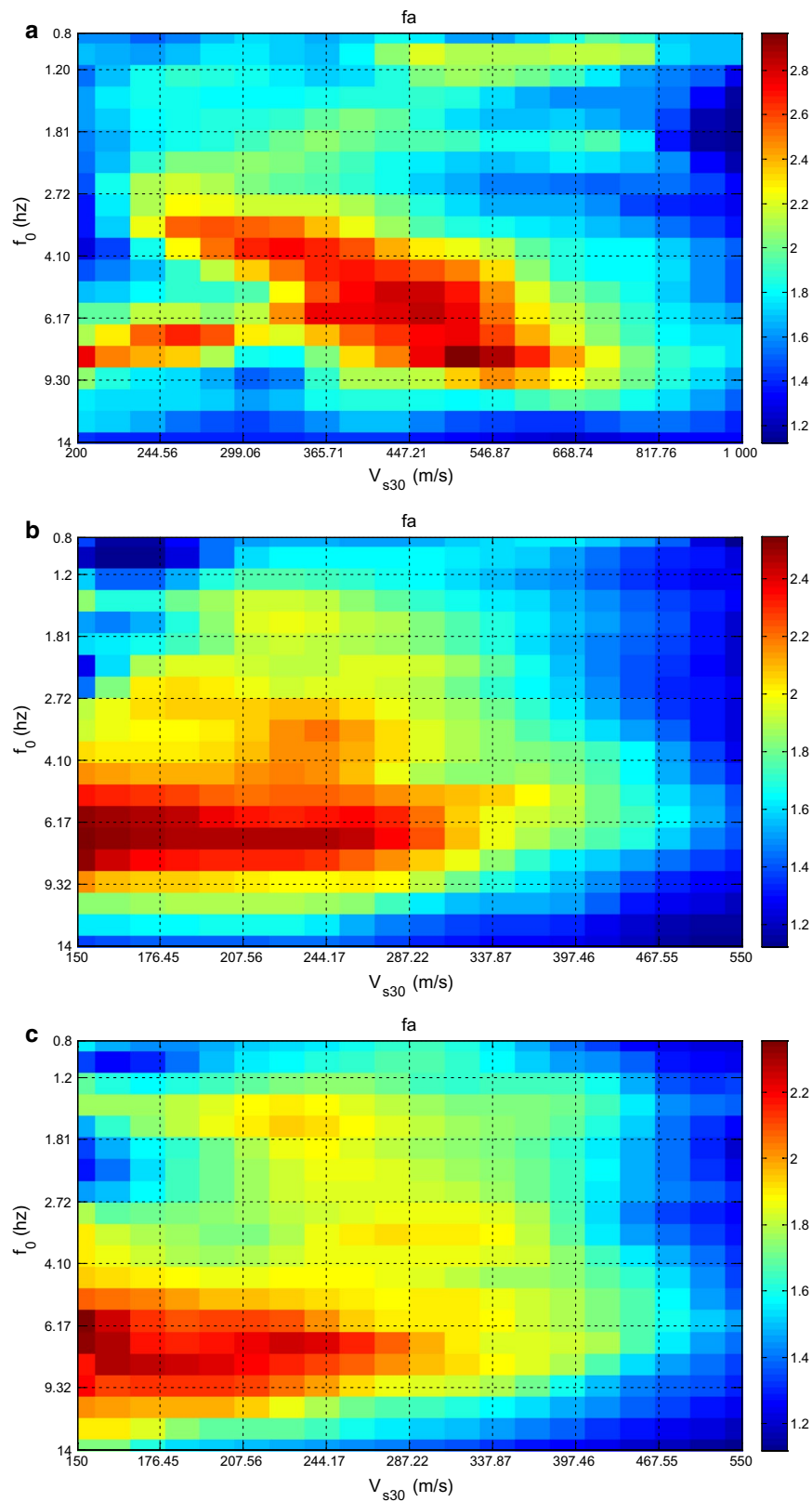


**Fig. 14** Variation in the short-period Borchardt factor  $F_a$  with  $V_{s30}$  (horizontal axis, log scale) and  $f_0$  (vertical axis, log scale) for RP-RF (a, top), NP-RF (b, middle), and TP-RF (c, bottom). Values of  $F_a$  are provided by the color scale on the right of each plot

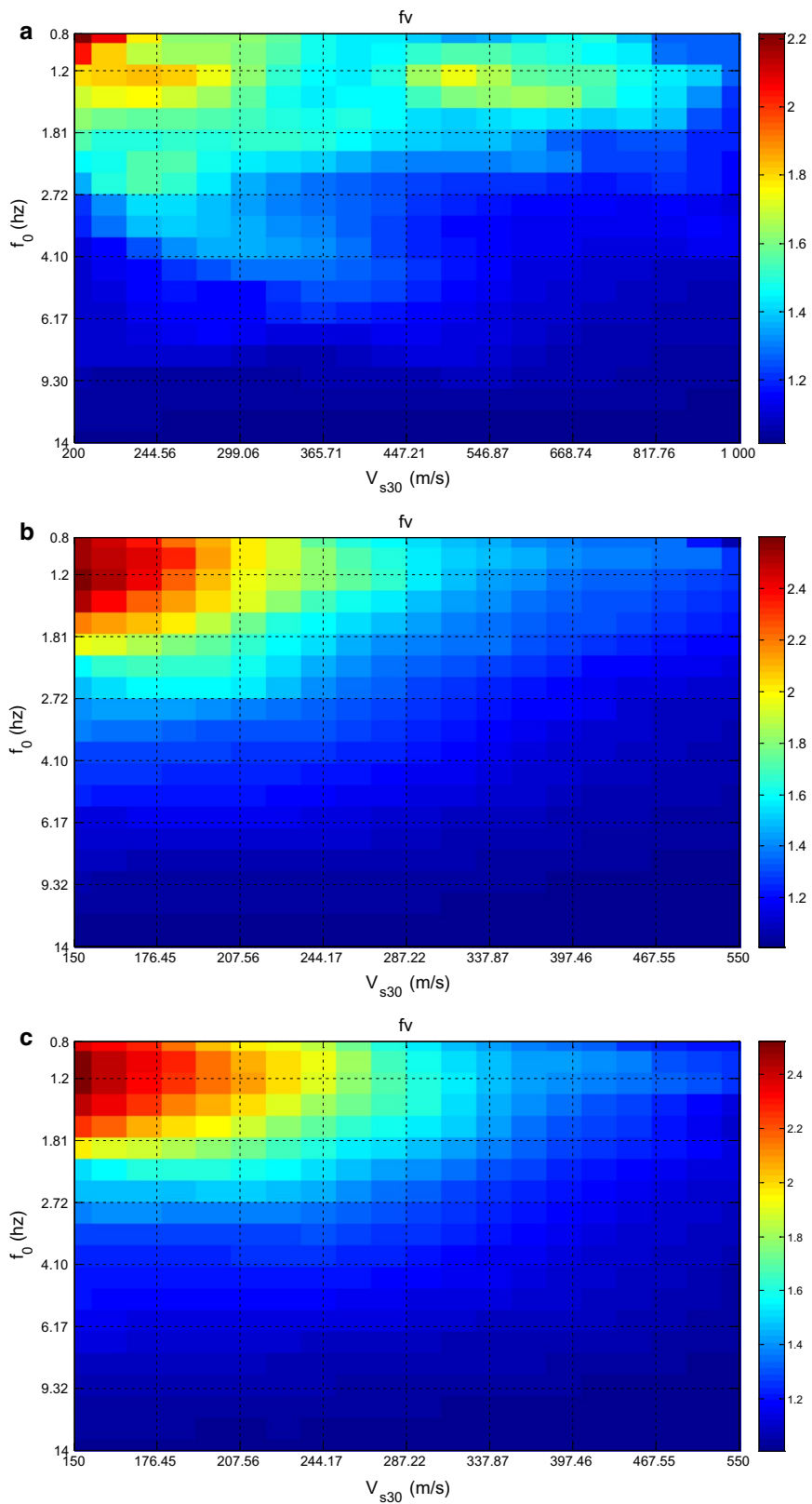


**Fig. 15** Variation in the mid-period Borcherdt factor  $F_v$  with  $V_{s30}$  (horizontal axis, log scale) and  $f_0$  (vertical axis, log scale) for RP-RF (a, top), NP-RF (b, middle), and TP-RF (c, bottom). Values of  $F_v$  are provided by the color scale on the right of each plot

fractile range of each considered explanatory parameter. The [0.8, 14 Hz] interval is considered for  $f_0$  in all cases, even though it would be possible to consider higher frequencies for the TP case. The considered  $V_{S30}$  interval is [200, 1000 m/s] for the RP case and [150, 550 m/s] for the NP and TP cases.

The corresponding distribution of soil profiles for any pair of site proxies ( $f_0$ ,  $V_{S30}$ ) is mapped in Fig. 16 for profile sets of RP, NP, and TP. This distribution is rather uniform in the two latter cases, while there is a lack of data in the RP set in the lower left and upper right corners. Therefore, the RP–RF model is poorly constrained for high-frequency, low-velocity sites (typically  $f_0 > 5$  Hz and  $V_{S30} < 350$  m/s) and for low-frequency, high-velocity sites (typically  $f_0 < 2$  Hz and  $V_{S30} > 600$  m/s).

The behavior of  $F_a$  and  $F_v$  with  $f_0$  and  $V_{S30}$  is expressed with the following explicit equation associated with the GRNN models:

$$\log(F_a) = \frac{\sum_{j=1}^Q (\log(F_{a,j}) w_j)}{\sum_{j=1}^Q w_j} \quad (29)$$

where  $w_j$  are the weights of each training data, estimated from their Euclidian distance in the  $(\log(f_0), \log(V_{S30}))$  plane ( $x_1 = \log(f_0)$  and  $x_2 = \log(V_{S30})$ )

$$w_j = \exp \left( - \left[ b \sqrt{[(\log(f_0) - \log(f_{0,j}))^2 + (\log(V_{S30} - \log(V_{S30,j}))^2]} \right]^2 \right) \quad (30)$$

and similar relationships for  $F_v$ .

The optimal  $b$  value is derived during the training phase and found to be equal to 16.65.

An Excel file is provided as an additional file for the practical use of these equations.

Generally, the short-period amplification factor  $F_a$  (Fig. 14) reaches the highest values for sites with intermediate to high fundamental frequency and low velocities at shallow depth. The maximum values exceed 2.5 for all cases, but correspond to slightly different ( $f_0$ ,  $V_{S30}$ ) combinations. Large  $F_a$  are found for the RP setup to  $V_{S30}$  values of 550 m/s (and corresponding fundamental frequencies around 6–9 Hz), while for the NP and TP sets, they are restricted to  $V_{S30}$  values below 300 m/s. Such differences are related to the possibility of high amplitude resonance when a thin layer of stiff soil is underlain by very hard rock, a situation that is quite frequent in real profiles. It is impossible in normalized or truncated profiles because of the velocity reduction imposed by the 800 m/s bedrock condition.

In parallel, the intermediate-period amplification factor  $F_v$  is found, as expected, to reach its highest values, above 2, for low-frequency and low-velocity sites:

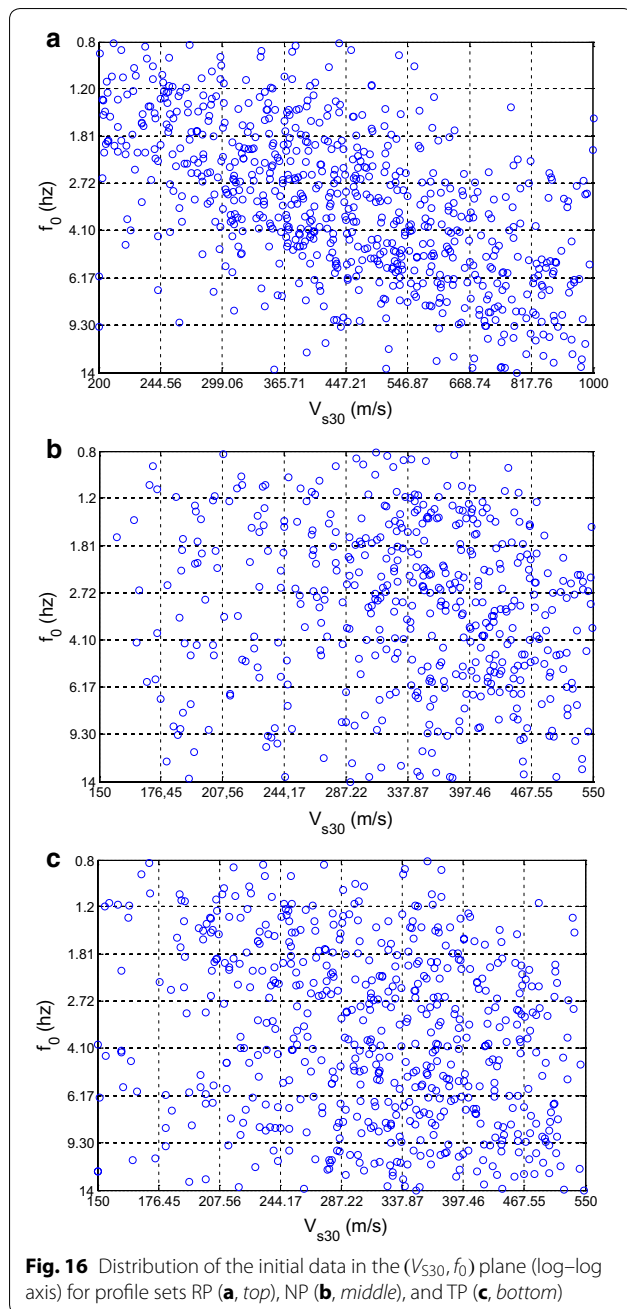
$f_0$  below 1.5–2 Hz,  $V_{S30}$  below 200 m/s (Fig. 15). Conversely,  $F_v$  remains small (below 1.4) for high-frequency sites ( $f_0$  beyond 4 Hz) for all values of  $V_{S30}$ . For RP, it may remain significant (between 1.4 and 1.6) for stiff sites ( $V_{S30} > 400$  m/s) and low frequency when the bedrock is deep and hard enough for the fundamental frequency to remain below 2 Hz. However, for NP and TP it is lower than 1.4 when  $V_{S30}$  exceeds 350 m/s.

Which among the RP–RF, NF–RF, and TP–RF relationships should be used for practical purposes? It should first be reminded that the present study only addresses the linear case as a preliminary, feasibility stage. This may explain for the relatively limited  $F_v$  values, which are often smaller than the  $F_a$  values. However, to obtain first-order estimates of  $F_a$  and  $F_v$  values for the linear response of a given site, the first step is to approximately identify the stiffness of underlying bedrock. For very hard bedrock, with S-wave velocities exceeding 1.2–1.5 km/s, it is better to select the RP–RF relationships. For bedrock that may be assumed to be close to a “standard” bedrock, with a S-wave velocity between 600 and 1000 m/s, and when  $V_{S30}$  value is below 550 m/s, it is probably preferable to select the NP–RF or TP–RF relationships. As shown in Fig. 16 (and Table 2), the

relationship may be considered reliable for the whole rectangular area described by the 5–95% fractile range of the two parameters for the NP and TP cases. In contrast, the RP model is poorly constrained for high-frequency, low-velocity sites and for low-frequency, high-velocity sites.

Finally, for the AF values, all possible combinations of site parameters are also considered, and associated GRNN models are derived and analyzed. The performances of some are listed in Tables 8, 9, 10, and the average performance of each considered site proxy is displayed in Fig. 17, similar to in Fig. 13, for the two parameters  $F_a$  and  $F_v$ .

As expected from previous results, one parameter performs almost systematically better than the others to explain the amplification factors, the velocity contrast  $C_v$ . However, it is superseded by the fundamental frequency for predicting  $F_v$  values in all three RP, NP, and TP cases, and  $f_0$  proves to be a very relevant parameter for intermediate- to long-period amplification. The widely used  $V_{S30}$  proxy performs better than the fundamental frequency  $f_0$  only for  $F_a$  and in the NP case, and the performance gain is only slight.



## Conclusions

The present study was a numerical investigation aiming at identifying the key parameters controlling 1D site response, starting with the linear domain as the first stage. For 858 soil columns corresponding to measured, real sites profiles from Japan, the USA, and Europe, the 1D linear (viscoelastic) response was computed for vertically incident plane waves and a representative set of

real input accelerograms spanning a wide range of peak frequencies. The geometric averages of the corresponding amplifications were derived from the ratio of surface to input acceleration response spectra, both in terms of frequency-dependent amplification factors  $AF(f)$  and in terms of “summary” short- and mid-period amplification factors  $F_a$  and  $F_v$ , averaged over period ranges [0.1 s, 0.2 s] and [0.75 s, 1.5 s], respectively. Generalized regression neural network (GRNN) models were used to investigate the relationships between these amplification factors and several “usual” site proxies, i.e.,  $V_{s30}$ ,  $f_0$ , sediment thickness, corresponding harmonic average sediment velocity, maximum velocity contrast, and bedrock velocity. Since real profiles exhibit a large site-to-site variability in bedrock velocity, two other sets of profiles with a constant bedrock velocity set to 800 m/s were considered. A common scaling was first applied to velocity and thickness values to normalize the real profiles to a uniform bedrock velocity of 800 m/s (without changing the transfer functions). The same real profiles were also truncated at the depth where their S-wave velocity first exceeded 800 m/s. GRNN models were then developed for these two additional sets of profiles. Many GRNN models were considered in each case, with all possible combinations of site proxies. This provided a mechanism for comparing the performances of every proxy to explain (and predict) site amplification.

The results showed that the key characteristics of the frequency-dependent  $AF$  may be satisfactorily reproduced with a limited number of site proxies. The best performing site parameter is the overall impedance contrast between bedrock velocity and minimum surface velocity. Because it is one of the most difficult and expensive parameters to measure, especially for thick deposits, other more convenient parameters are preferred, among them, the couple  $(V_{s30}, f_0)$  reduced the variance of residuals by at least 60%. From a code perspective, equations and plots were provided describing the dependence of the short- and mid-period amplification factors  $F_a$  and  $F_v$  on these two parameters.  $F_a$  reached its highest value for sites presenting simultaneously low velocities and high  $f_0$  values (i.e., thin, soft sites), while the largest values of  $F_a$  corresponded to low velocities and low  $f_0$  values.

These results open the way for improvements in site classification with a physical relationship between site proxies and site amplification. However, this work is only a first step, and the present results should be complemented with further investigations.

- First, the set of considered soil profiles is dominated by KiK-net sites, which are rather stiff. Although this bias was somewhat corrected with the set of “nor-



**Table 8 Evolution of the standard deviation of residuals for various GRNN models predicting  $F_a$  and  $F_v$  in the RP–RF case**

Number of parameters	Explanatory parameters	$F_a$		$F_v$	
		Standard deviation of residuals	Variance reduction	Standard deviation of residuals	Variance reduction
All (6)	Depth + $f_0 + V_{sm} + C_v + V_{s30} + V_{bed-rock}$	0.0020	99.9%	0.00023	99.9%
3 (best triplet)	$f_0 + C_v + V_{s30}$	0.0094	99.6%	0.0067	99.5%
2 (best pair)	$f_0 + C_v$	0.0349	94.9%	0.0173	97.0%
2 (convenient pair)	$f_0 + V_{s30}$	0.1083	50.7%	0.0515	73.2%
1 (best for $F_a$ )	$C_v$	0.0878	67.6%	0.0786	37.6%
1 (best for $F_v$ )	$f_0$	0.1355	22.9%	0.0661	55.9%
1 (usual)	$V_{s30}$	0.1419	15.4%	0.0752	42.9%
Initial $\sigma$		0.1543		0.0995	

**Table 9 Evolution of the standard deviation of residuals for various GRNN models predicting  $F_a$  and  $F_v$  in the NP–RF case**

Normalized profiles		$F_a$		$F_v$	
Number of parameters	Explanatory parameters	Standard deviation of residuals	Variance reduction	Standard deviation of residuals	Variance reduction
All (5)	Depth + $f_0 + V_{sm} + C_v + V_{s30}$	0.0055	99.74%	0.0011	99.98%
3 (best triplet)	$f_0 + C_v + V_{s30}$	0.012	98.7%	0.0034	99.8%
2 (best pair for $F_a$ )	$f_0 + C_v$	0.0318	91.43%	0.0172	95.7%
2 (convenient pair)	$f_0 + V_{s30}$	0.0592	70.28%	0.0153	96.6%
1 (best for $F_a$ )	$C_v$	0.0783	48.02%	0.0733	21.8%
1 (best for $F_v$ )	$f_0$	0.0944	24.44%	0.048	66.4%
1 (usual)	$V_{s30}$	0.0926	27.3%	0.0709	26.8%
Initial $\sigma$		0.1086		0.0829	

**Table 10 Evolution of the standard deviation of residuals for various GRNN models predicting  $F_a$  and  $F_v$  in the TP–RF case**

Truncated profiles		$F_a$		$F_v$	
Number of parameters	Explanatory parameters	Standard deviation of residuals	Variance reduction	Standard deviation of residuals	Variance reduction
All 5	Depth + $f_0 + V_{smn} + C_v + V_{s30}$	0.0095	99.28%	0.0017	99.97%
3 (best triplet)	$f_0 + C_v + V_{s30}$	0.0185	97.2%	0.0061	99.57%
2 (best pair for $F_a$ )	$f_0 + C_v$	0.0375	88.8%	0.0229	93.9%
2 (convenient pair)	$f_0 + V_{s30}$	0.0511	79.1%	0.0127	98.1%
1 (best, $F_a$ )	$C_v$	0.0734	57.05%	0.0736	37.9%
1 (best, $F_v$ )	$f_0$	0.0764	53.47%	0.0428	79%
1 (usual)	$V_{s30}$	0.0925	31.4%	0.0777	30.8%
Initial $\sigma$		0.112		0.0934	

malized profiles” or “truncated profiles,” it is not fully satisfactory because the normalization procedure also included a depth scaling to maintain unchanged

frequencies. Adding softer sites would extend the applicability range of the results to softer and thicker sites.

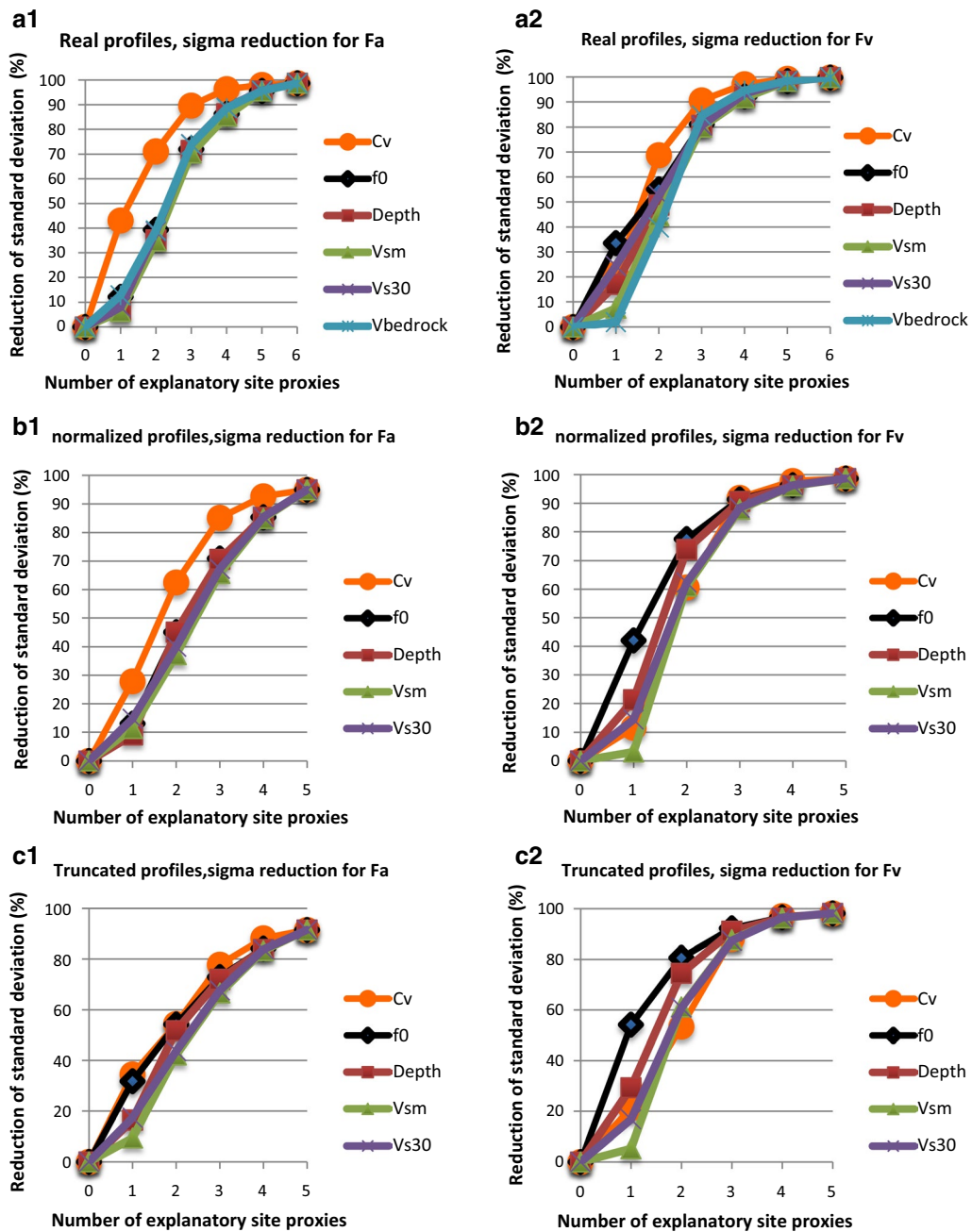


**Fig. 17** Performance indicators for Borcherdt factors prediction models based on the reduction in the standard deviation of residuals  $RS_m$  for various site proxies (different curves) for RP-RF (a, top), NP-RF (b, middle), and TP-RF (c, bottom). The left column (1) corresponds to  $F_a$  models, and the right one (2) corresponds to  $F_v$  models. The display is similar to that presented in Fig. 13

- Second, these results are limited to the linear case. An important next step will be to consider nonlinear site responses. Assigning nonlinear characteristics to different layers of each soil pro-

file (information that is presently unavailable) and adding at least one explanatory variable in the input layer, related to the loading level, will be required.

## Additional files

**Additional file 1.** Distribution of the site parameters for the “real profiles” (RP) set

**Additional file 2.** Distribution of the site parameters for the “normalized Profiles”

**Additional file 3.** Distribution of the site parameters for the “truncated profiles”

**Additional file 4.** Analog to Fig. 13 for the normalized frequency domain: (reduction in standard deviation  $RS_m$ ) for the various site proxies (different curves) for RP–NF (a, top), NP–NF (b, middle), and TP–NF (c, bottom)

**Additional file 5.** Excel sheet to estimate the short- and mid-period amplification factors  $F_a$  and  $F_v$  based on  $V_{530}$  and  $f_0$  values for RP–RF

## Abbreviations

AF: amplification factor (ratio of site to “reference rock” acceleration response spectrum with 5% damping);  $C_v$ : velocity contrast between bedrock and the softest layers, which is generally at the surface, but not systematically; Depth: thickness down to the deepest (and hardest) geological unit;  $f_0$ : resonance frequency;  $F_a$ : amplification factor at short period (computed as the geometrical mean of AF for periods equally spaced on a logarithmic axis in the range [0.1 s, 0.2 s]);  $F_v$ : amplification factor at mid-period (computed as the geometrical mean of AF for periods equally spaced on a logarithmic axis in the range [0.75 s, 1.5 s]); GMPEs: ground motion prediction equations; GRNN: generalized regression neural network;  $h_i$ : thickness of layer  $i$ ; Mw: moment magnitude; RP: real profiles; NP: normalized profiles; TP: truncated profiles; NF: normalized frequency; RF: real frequency; PGA: peak ground acceleration; PSA: pseudo acceleration spectrum;  $Q_i$ : quality factor for layer  $i$ ;  $R^2$ : coefficient of determination;  $SA(T)_i$ : 5% response spectra at the outcropping reference bedrock;  $SA(T)_s$ : 5% response spectra at the site surface;  $V_i$ : shear wave velocity for layer  $i$ ;  $V_{\text{Bedrock}}$ : shear wave velocity of bedrock;  $V_{530}$ : harmonic average of the shear wave velocity over the topmost 30 m;  $V_{sm}$ : harmonic average of shear wave velocity over the total soil column thickness;  $\xi_i$ : damping of layer  $i$ ;  $\rho_i$ : mass density for layer  $i$ .

## Authors' contributions

Most scientific and technical work was conducted by the first author (Ahmed Boudghene Stambouli), under the scientific supervision of the three other coauthors. The preparation and editing of the manuscript were shared between the three first authors. All authors read and approved the final manuscript.

## Author details

<sup>1</sup> Risk Assessment and Management Laboratory (RISAM), Faculté de Technologie, Université Abou Bekr Belkaid, BP 230-13048, Tlemcen, Algeria. <sup>2</sup> Institut de Sciences de la Terre (ISTerre), Maison des Géosciences, Université Grenoble-Alpes, IFSTTAR, Bâtiment OSUG C, CS 40700, 38058 Grenoble Cedex 9, France.

## Acknowledgements

This work was partially supported by the project: “Prédiction du mouvement sismique et estimation du risque sismique lié aux effets de site” 13MDU901 Tassili CMEP between Universities of Tlemcen (Algeria) and Grenoble (France). The authors wish to express their acknowledgment for this support. They wish also to acknowledge the contribution of C. Cornou from ISTerre (U. Grenoble) and D. Boore from the USA Geologic Survey who provided data for the 858 soil profiles. We also thank Dr. Sanjay Singh Bora and an anonymous reviewer for their careful reading and helpful comments and suggestions that have greatly contributed to clarify several issues and improved the final version. The final editing largely benefitted from the Earth, Planets, and Space journal services.

## Competing interests

The authors declare they have no competing interests.

## Availability of data and materials

The RP profile set was originally compiled by C. Cornou (Salameh 2016) and consists of about 600 Japanese KiK-net sites, more than 200 sites from the USA, made available by D. Boore (<http://quake.usgs.gov/~boore>), and 22 European sites measured during the NERIES project (Di Giulio et al. 2012). The KiK-net velocity profiles were directly obtained from <http://www.kyoshin.bosai.go.jp> and consist of surface-to-downhole measurements of S- and P-wave velocities.

## Publisher's Note

Springer Nature remains neutral with regard to jurisdictional claims in published maps and institutional affiliations.

Received: 28 November 2016 Accepted: 14 July 2017

Published online: 24 July 2017

## References

- Abrahamson N, Atkinson G, Boore D, Bozorgnia Y, Campbell K, Chiou B, Idriss I, Silva W, Youngs R (2008) Comparisons of the NGA ground-motion relations. *Earthq Spectra* 24(1):45–66
- Aki K, Richards PG (1980) Quantitative seismology, theory and methods, vol 1. WH Freeman & Co., New York
- Akkar S, Sandikkaya MA, Şenyurt M, Sisi AA, Ay BÖ, Traversa P, Godey S (2014) Reference database for seismic ground-motion in Europe (RESORCE). *Bull Earthq Eng* 12(1):311–339
- Almakari M, Régnier J, Salameh C, Cadet H, Bard PY, Lopez-Caballero F, Cornou C (2016) Modulation of weak motion site transfer functions by non-linear behavior: a statistical comparison of 1D numerical simulation with KiK-net data. In: Proceedings of the 5th IASPEI/IAEE international symposium: effects of surface geology on seismic motion, Taipei, August 15–17 Paper P101C, 14 pp
- Ancheta TD, Darragh RB, Stewart JP, Seyhan E, Silva WJ, Chiou BS-J, Wooddell KE, Graves RW, Kottke AR, Boore DM, Kishida T, Donahue JL (2014) NGA-West 2 database. *Earthq Spectra* 30:989–1005
- Anderson JG, Bodin P, Brune JN, Prince J, Singh SK, Quaas R, Onate M (1986) Strong ground motion from the Michoacan, Mexico, earthquake. *Science* 233(1043):9
- Bard P-Y, Campillo M, Chavez-Garcia FJ, Sanchez-Sesma FJ (1988) The Mexico earthquake of September 19, 1985—a theoretical investigation of large- and small-scale amplification effects in the Mexico City Valley. *Earthq Spectra* 4(3):609–633. doi:10.1193/1.1585493
- Bardet JP, Ichii K, Lin CH (2000) EERA: a computer program for equivalent-linear earthquake site response analyses of layered soil deposits. University of Southern California, Department of Civil Engineering
- Biro Y, Renault P (2012) Importance and impact of host-to-target conversions for ground motion prediction equations in PSHA. In: Proceedings of the 15th world conference on earthquake engineering, pp 24–28
- Bora SS, Scherbaum F, Kuehn N, Stafford P, Edwards B (2015) Development of a response spectral ground-motion prediction equation (GMPE) for seismic-hazard analysis from empirical fourier spectral and duration models. *Bull Seism Soc Am* 105(4):2192–2218
- Bora SS, Scherbaum F, Kuehn N, Stafford P (2016) On the relationship between fourier and response spectra: implications for the adjustment of empirical ground-motion prediction equations (GMPEs). *Bull Seism Soc Am* 106(3):1235–1253
- Borcherdt RD (1994) Estimates of site dependent response spectra for design (methodology and justification). *Earthq Spectra* 10:617–653
- Borcherdt RD (2002) Empirical evidence for acceleration-dependent amplification factors. *Bull Seism Soc Am* 92(2):761–782
- Cadet H, Bard P-Y, Duval A-M, Bertrand E (2012) Site effect assessment using KiK-net data—part 2—site amplification prediction equation (SAPE) based on  $f_0$  and  $V_{sz}$ . *Bull Earthq Eng* 10:451–489
- Castellaro S, Mulargia F, Rossi PM (2008) Vs30: proxy for seismic amplification? *Seism Res Lett* 79:540–543

- Chávez-García FJ, Bard PY (1994) Site effects in Mexico City eight years after the September 1985 Michoacan earthquakes. *Soil Dyn Earthq Eng* 13(4):229–247
- Cigizoglu HK, Alp M (2005) Generalized regression neural network in modeling river sediment yield. *Adv Eng Softw* 37:63–68
- Cruz-Atienza VM, Tago J, Sanabria-Gómez JD, Chaljub E, Etienne V, Virieux J, Quintanar L (2016) Long duration of ground motion in the paradigmatic valley of Mexico. *Sci Rep* 6:38807
- Derras B, Bard PY, Cotton F, Bekkouche A (2012) Adapting the neural network approach to PGA prediction: an example based on the KiK-net data. *Bull Seism Soc Am* 102(4):1446–1461
- Derras B, Bard PY, Cotton F (2014) Towards fully data driven ground-motion prediction models for Europe. *Bull Earthq Eng* 12(1):495–516. doi:10.1007/s10518-013-9481-0
- Derras B, Bard P-Y, Cotton F (2016) Site-conditions proxies, ground-motion variability and data-driven GMPs. Insights from NGA-West 2 and RESORCE datasets. *Earthq Spectra* 32(4):2027–2056
- Di Giulio G, Savvaidis A, Ohrnberger M, Wathelet M, Cornou C, Knapmeyer-Endrun B, Renalier F, Theodoulidis N, Bard P-Y (2012) Exploring the model space and ranking a best class of models in surface-wave dispersion inversion: application at European strong motion sites. *Geophysics* 77:B147
- Dickenson SE, Seed RB (1996) Nonlinear dynamic response of soft and deep cohesive soil deposits. In: Proceedings of the international workshop on site response subjected to strong earthquake motions, vol 2, pp 67–81
- Dobry R, Oweis I, Urzua A (1976) Simplified procedures for estimating the fundamental period of a soil profile. *Bull Seism Soc Am* 66(4):1293–1321
- Dobry R, Borcherdt RD, Crouse CB, Idriss IM, Joyner WN, Martin GR, Power MS, Rinne EE, Seed RB (2000) New Site coefficients and site classification system used in recent building seismic code provisions. *Earthq Spectra* 16(1):41–67
- Douglas J, Akkar S, Ameri G, Bard P-Y, Bindi D, Bommer JJ, Singh Bora S, Cotton F, Derras B, Hermskes M, Kuehn NM, Luzi L, Massa M, Pacor F, Riggelsen C, Sandikkaya MA, Scherbaum F, Stafford PJ, Traversa P (2014) Comparisons among the five ground-motion models developed using RESORCE for the prediction of response spectral accelerations due to earthquakes in Europe and the Middle East. *Bull Earthq Eng* 12(1):341–358. doi:10.1007/s10518-013-9522-8
- EC8 Eurocode 8 (2004). Design of structures for earthquake resistance—Part 1: general rules, seismic actions and rules for buildings. European Committee for Standardization (CEN), EN 1998-1, eurocodes.jrc.eceuropa.eu/. Last accessed Feb 2016
- Esteva L (1988) The Mexico earthquake of September 19, 1985—consequences, lessons, and impact on research and practice. *Earthq Spectra* 4:413–426
- Fukushima Y, Gariel JC, Tanaka R (1995) Site-dependent attenuation relations of seismic motion parameters at depth using borehole data. *Bull Seism Soc Am* 85(6):1790–1804
- Ghaboussi J, Lin CCJ (1998) New method of generating spectrum compatible accelerograms using neural networks. *Earthq Eng Struct Dyn* 27:377–396
- Giacinto G, Paolucci R, Roli F (1997) Application of neural networks and statistical pattern recognition algorithms to earthquake risk evaluation. *Pattern Rec Lett* 18:1353–1362
- Gregor N, Abrahamson NA, Atkinson GM, Boore DM, Bozorgnia Y, Campbell KW, Brian Chiou BS-J, Idriss IM, Kamai R, Seyhan E, Silva W, Stewart JP, Youngs R (2014) Comparison of NGA-West2 GMPs. *Earthq Spectra* 30(3):1179–1197
- Hall JF, Beck JL (1986) Structural damage in Mexico City. *Geophys Res Lett* 13(6):589–592
- Hannan SA, Manza RR, Ramteke RJ (2010) Generalized regression neural network and radial basis function for heart disease diagnosis. *Int J Comp App* 7(13):7–13
- Hashash YMA, Groholski DR, Phillips CA, Park D, Musgrove M (2012) DEEPSOIL 5.1, user manual and tutorial. Department of Civil and Environmental Engineering, University of Illinois at Urbana-Champaign
- Haskell NA (1953) The dispersion of surface waves on multilayered media. *Bull Seism Soc Am* 43:17–34
- IBC (2012) International Building Code 2012 Edition, ISBN 978-1-60983-039-7, International Code Council, Washington. <https://archive.org/details/gov.law.icc.ibc.2012>. Last accessed Nov 2016
- Kawase H, Aki K (1989) A study on the response of a soft soil basin for incident S, P, and Rayleigh waves with special reference to the long duration observed in Mexico City. *Bull Seism Soc Am* 79:1361–1382
- Kim B, Lee DW, Parka KY, Choi SR, Choi S (2004) Prediction of plasma etching using a randomized generalized regression neural network. *Vacuum* 76:37–43
- Kramer SL (1996) Geotechnical earthquake engineering. Pearson Education India, New Delhi
- Lin CCJ, Ghaboussi J (2001) Generating multiple spectrum compatible accelerograms using stochastic neural networks. *Earthq Eng Struct Dyn* 30:1021–1042
- Luzi L, Puglia R, Pacor F, Gallipoli MR, Bindi D, Mucciarelli M (2011) Proposal for a soil classification based on parameters alternative or complementary to Vs, 30. *Bull Earthq Eng* 9(6):1877–1898
- Martin GR, Dobry R (1994) Earthquake site response and seismic code provisions. *NCEER Bull* 8(4):1–6
- Paolucci R, Colli P, Giacinto G (2000) Assessment of seismic site effect in 2-D alluvial valleys using neural networks. *Earthq Spectra* 16:661–680
- Pitilakis KD, Makra KA, Raptakis DG (2001) 2D vs 3D site effects with potential applications to seismic norms: the case of EUROSEISTEST and Thessaloniki. In: Proceedings of the XVth ICSMGE, Istanbul, pp 123–133
- Pitilakis K, Riga E, Anastasiadis A (2012) Design spectra and amplification factors for Eurocode 8. *Bull Earthq Eng* 10(5):1377–1400
- Pitilakis K, Riga E, Anastasiadis A (2013) New code site classification, amplification factors and normalized response spectra based on a worldwide ground-motion database. *Bull Earthq Eng* 11(4):925–966
- Renault PLA, Abrahamson NA, Bard P-Y, Fäh D, Pecker A, Studer J (2014) PEGA-SOS Refinement Project, volume 5, SP3 - Site Response Characterization, 672 pp. Available from <http://www.swissnuclear.ch/de/downloads.html>. ©2013–2015 Swissnuclear, Olten
- Rodríguez-Marek A, Bray JD, Abrahamson NA (2001) An empirical geotechnical seismic site response procedure. *Earthq Spectra* 17(1):65–87
- Romo MP, Jaime A, Resendiz D (1988) General soil conditions and clay properties in the Valley of Mexico. *Earthq Spectra* 4:731–752
- Salameh C (2016) Ambient vibrations, spectral contents and seismic damage: a new approach adapted to urban scale. Application to Beirut (Lebanon). PhD thesis, University Grenoble-Alpes, France, defended on June 21, 2016 (284 pp, in English)
- Salameh C, Bard P-Y, Guillier B, Harb J, Cornou C, Gérard J, Almakari M (2017) Using ambient vibration measurements for risk assessment at an urban scale: from numerical proof of concept to Beirut case study (Lebanon). *Earth Plan Space* 69:60. doi:10.1186/s40623-017-0641-3
- Sanchez-Sesma F, Chavez-Perez S, Suarez M, Bravo MA, Perez-Rocha LE (1988) On the seismic response of the Valley of Mexico. *Earthq Spectra* 4:569–589
- Schnabel PB, Lysmer J, Seed HB (1973). SHAKE—a computer program for earthquake response analysis of horizontally layered sites, Report No, EERC 72 12, Earthquake Engineering Research Center, University of California, Berkeley
- Seed HB, Romo MP, Sun JI, Jaime A, Lysmer J (1988) Relationships between soil conditions and earthquake ground motions. *Earthq Spectra* 4:687–729
- Singh SK, Ordaz M (1993) On the Origin of long coda observed in the lake-bed strong-motion records of Mexico City. *Bull Seism Soc Am* 83:1298–1306
- Singh SK, Lermo J, Dominguez T, Ordaz M, Espinosa JM, Mena E, Quaaas R (1988a) The Mexico earthquake of September 19, 1985—a study of amplification of seismic waves in the valley of Mexico with respect to a hill zone site. *Earthq Spectra* 4(4):653–673
- Singh SK, Mena EA, Castro R (1988b) Some aspects of source characteristics of the 19 September 1985 Michoacan earthquake and ground motion amplification in and near Mexico City from strong motion data. *Bull Seism Soc Am* 78(2):451–477
- Specht DF (1991) A general regression neural network. *IEEE Trans Neural Netw* 2(6):568–576
- Thomson WT (1950) Transmission of elastic waves through a stratified solid medium. *J Appl Phys* 21:89–93
- Uniform Building Code (1997) Structural engineering design provisions. In: International conference of building officials, vol 2
- Wasserman PD (1993) Advanced methods in neural computing. Wiley, New York